

1 **Insights and Comparison of Structure–Bulk Property Relationships in Low**
2 **Generation Hydroxylated Polyester Dendrimer and Hyperbranched Polymer**
3 **Prepared from bis-MPA Monomer**

5 *Beibei Chen^a, Maliha N. Syed^a, Samantha P. Daymon^a, Brian G. Olson^a, Oluwapelumi O.*
6 *Kareem^b, Joseph A. Giesen^b, Gregory B. Fahs^c, Robert R. Moore^c, Scott M. Grayson^b, Sergei*
7 *Nazarenko^a**

9 ^a*School of Polymer Science and Engineering, University of Southern Mississippi, Hattiesburg,*
10 *MS 39406, United States*

11 ^b*Department of Chemistry, Tulane University, New Orleans, Louisiana 70118, United States*

12 ^c*Department of Chemistry, Virginia Tech, Blacksburg, VA 24061, United States*

14 *Corresponding author: Sergei.Nazarenko@usm.edu Tel.: 601 266 5967; fax: 601 266 5504

16 Keywords: bis-MPA, dendrimers; hyperbranched polymers; characterization; structure-property
17 relationships; PVT, Simha-Somcynsky (S-S) equation of state; free volume;

19 August 10, 2021

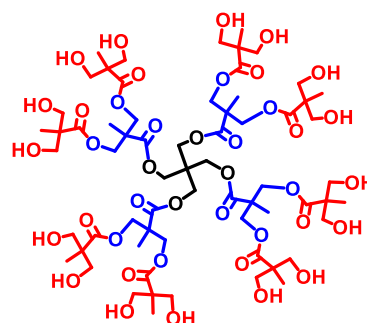
20 **ABSTRACT**

21 In this study a second generation, perfectly branched dendrimer (D2) was synthesized
22 using an iterative method via anhydride coupling from a bis-MPA monomer and a
23 pentaerythritol core. The multigram scale production of this dendrimer in the lab enabled a
24 multifaceted investigation of structure-bulk property relationships and a subsequent comparison
25 with those of the second generation of a chemically similar but hyperbranched polymer (HBP2)
26 produced via rapid one-pot synthesis from a bis-MPA monomer and an ethoxylated
27 pentaerythritol core. Several characterization tools such as ¹H NMR, FTIR, DSC, WAXS, and
28 high-pressure dilatometry were employed to explicate fundamental differences and similarities
29 between these two important dendritic polymer subclasses. Specifically, high pressure
30 dilatometry permitted an investigation of temperature and pressure effects on specific volume

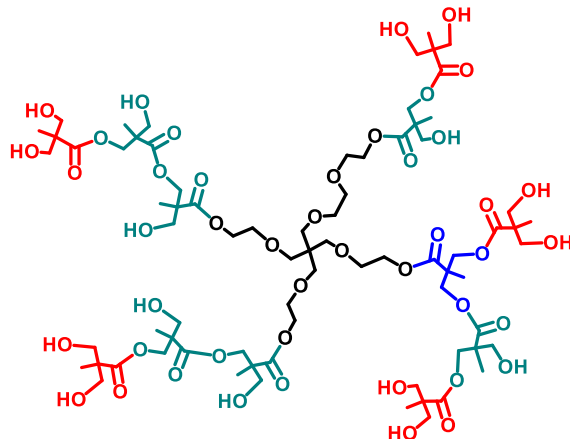
1 (PVT) of the dendrimer and its HBP analogue. Fitting PVT data to the Simha-Somcynsky (S-S)
 2 equation of state (EOS) for the melt state enabled demonstration the power of this EOS,
 3 originally developed for linear polymers, to also fully describe the PVT surfaces of the
 4 dendrimer and HBP in this study. Generated molecular parameters from the S-S model were
 5 compared with those for other polymeric systems. Finally, fractional free volume for the
 6 dendrimer and HBP, determined from the PVT data and the S-S model, at various temperatures
 7 and pressures was compared.

TOC

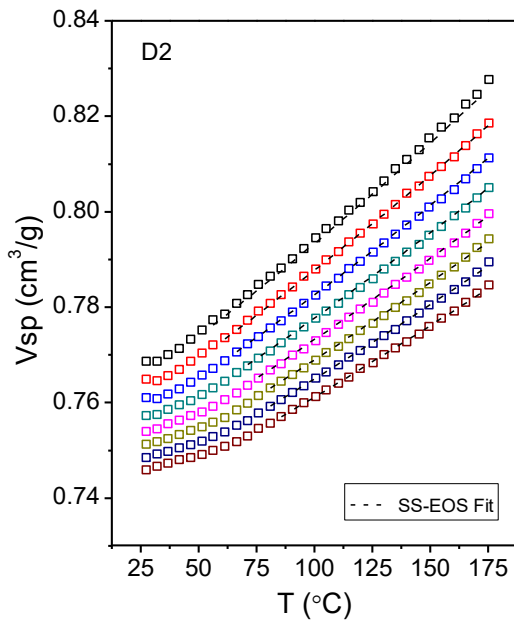
2nd Generation Dendrimer



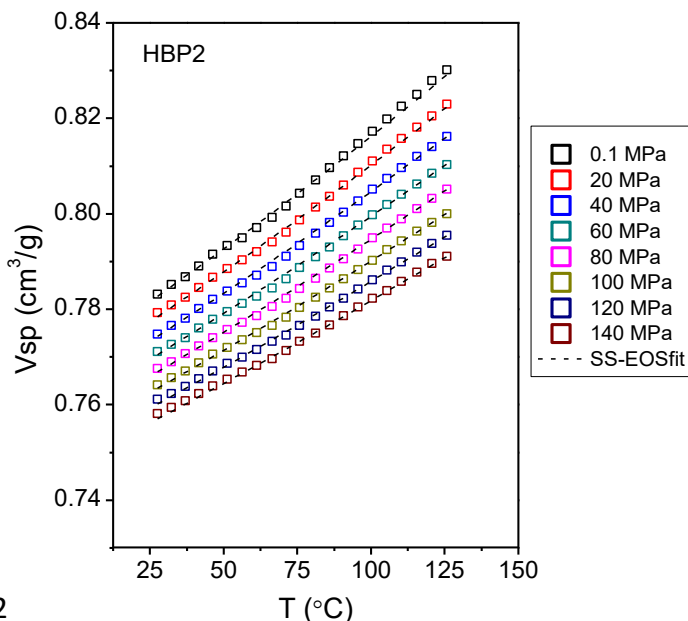
2nd Pseudogeneration HBP



D2



HBP2



1 INTRODUCTION

2 Among an array of dendritic structures that have been reported, dendrimers (Ds) and
3 hyperbranched polymers (HBPs) are the two most recognizable subclasses [1,2]. General
4 prominent features of both Ds and HBPs include a central core, an exterior surface composed of
5 numerous functional groups, and the interior structure which can be enlarged by adding more
6 layers or generations (pseudo-generations in HBPs) of repeat units. Dendrimers are fully
7 branched and monodisperse macromolecules while HBPs are partially branched and
8 polydisperse. Compared to monodisperse dendrimers, which require more laborious, iterative
9 synthesis, HBPs are becoming increasingly attractive in an attempt to develop polymeric systems
10 with properties comparable to dendrimers but using more facile and economic synthetic methods
11 [3,4]. In particular, with regard to the synthesis of hyperbranched polyesters, two basic synthetic
12 approaches should be noted: polycondensation of one type, AB_x ; and branching monomers and
13 polycondensation which employs two different, mutually reactive, multifunctional monomers A_x
14 and B_y . Note, either x or y must be greater than 2 [5–7]. A distinct feature of the HBP structure is
15 the inclusion of linear units (imperfections resulting from partial reaction) which situate end-
16 groups throughout the structure, as opposed to solely at the periphery as in dendrimers.
17 Understanding the significance of linear sequences may not only lead to a deeper understanding
18 of dendritic architectures, but also explain the different physical properties of HBPs as compared
19 to their dendrimer counterparts [8,9].

20 One of the most widely employed families of dendritic polymers utilize 2,2-
21 bis(hydroxymethyl)propionic acid (bis-MPA) as a branching monomer [10,11]. An efficient and
22 commercially viable synthesis has been proposed for bis-MPA based HBPs using a one-pot
23 method [12,13]. For the synthesis of bis-MPA based dendrimers, two methods have been
24 proposed: the double-stage convergent approach [14], and the divergent approach by anhydride
25 coupling [15]. Although a protocol has been established to make high purity dendrimers on a
26 gram scale, no such protocol suitable for industrial scale production of bis-MPA Ds has been
27 found. Meanwhile, bis-MPA based HBPs have been commercialized since the early 1990s and
28 sold to the market by Perstorp AB under the trade name BoltornTM. More recently Polymer
29 Factory in Sweden AB and Sigma Aldrich Corporation have also contributed to their widespread
30 use. BoltornTM HBPs find applications as crosslinkers, cure and toughening agents, drug carriers,

1 matrices for hybrid materials and composites, multifunctional components in coating and resin
2 formulations and many others [16].

3 Mainly due to commercial availability, bis-MPA based Boltorn® HBPs, pseudo -
4 generations (2-5), have been employed in several studies aiming to elucidate the structure-
5 property relationships in the bulk [10]. It was discovered that many bulk properties of bis-MPA
6 HBPs are largely governed by the ability of these rather low molecular weight macromolecules
7 to form hydrogen bonds (H-bonds), both intra- and intermolecularly, primarily via association of
8 numerous hydroxyl groups with each other and/or with carbonyl, ester, and ether oxygen atoms
9 forming H-bond networks. This was most vividly demonstrated in the past by functionalizing the
10 hydroxyl groups of bis-MPA based HBPs with non-hydrogen bonding moieties. The glass
11 transition temperature (T_g) of an HBP modified either with propionate, benzoate, or aliphatic
12 end-groups were dramatically lower than those of the unmodified, hydroxylated HBP.
13 Additionally, most Boltorn® HBPs are solid at room temperature, but after being end-capped
14 with short alkyl chains become fluid [17].

15 Due to limited availability of bis-MPA based dendrimers, systematic and comprehensive
16 studies comparing the bulk properties of bis-MPA HBPs with those of dendrimer analogues
17 ~~barely exist~~ are rare. It has been claimed that the fourth generation bis-MPA based HBP
18 exhibited a tendency to structurally order in the bulk while the dendrimer of the same generation
19 did not [18].

20 The purpose of this study was to conduct a thorough structure-bulk property comparison
21 between the second generation bis-MPA based perfect dendrimer synthesized for this study on a
22 multigram scale and the second generation of a chemically similar but hyperbranched polymer.
23 An array of molecular and structural characterization tools such as ^1H NMR, FTIR, DSC, WAXS
24 and high-pressure dilatometry (PVT) was used in this study to elucidate the fundamental
25 differences and similarities between these two important dendritic polymer subclasses.

26 **EXPERIMENTAL**

27 **Materials and sample preparation**

28 The Boltorn™ second (H20) pseudo-generation bis-MPA based hyperbranched polymers
29 (HBP) was donated by Perstorp Polyols Inc., Sweden. In the commercial abbreviation HX0, X

1 denotes the pseudo-generation number (second in this case). Hereafter H20 HBP will be
 2 designated in this article as HBP2. Perstorp reports an average molecular weight for HBP2 as

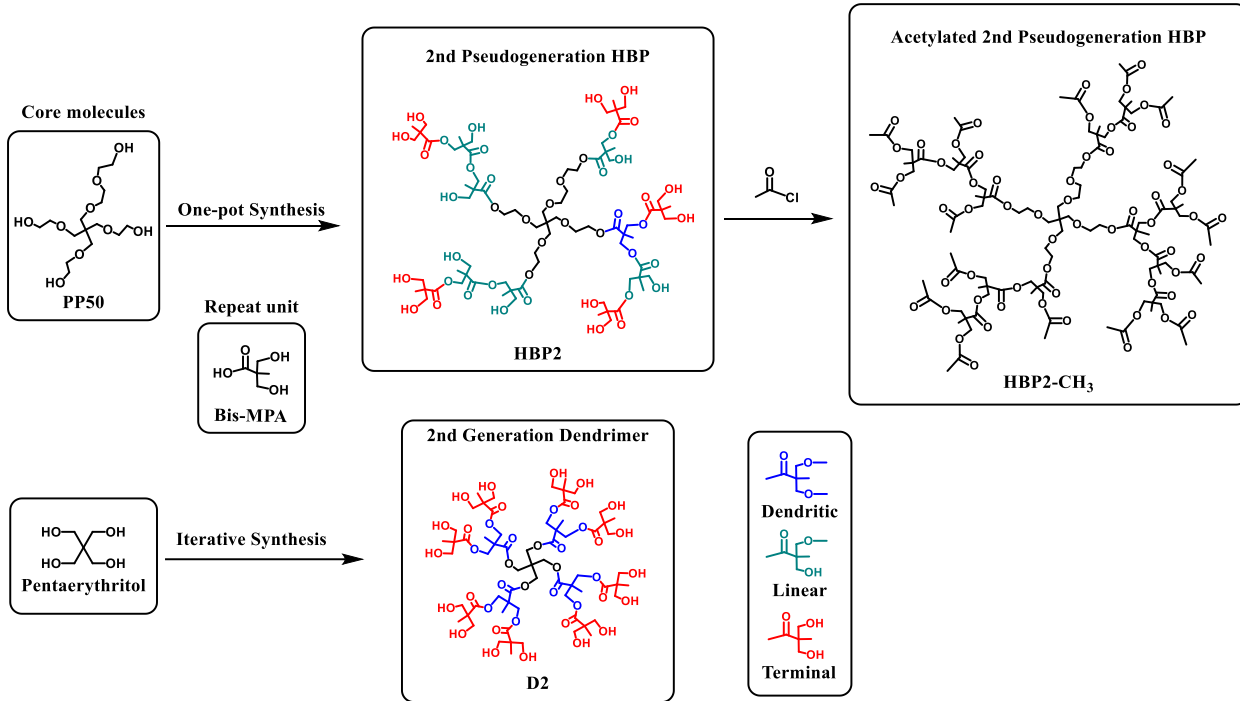


Figure 1. Skeletal formulae of chemical components and polymers described in this manuscript. Dendritic (D), terminal (T), and linear (L) structural unit types for D2 and HBP2 systems are shown in different colors to help an eye.

3 2100 g/mol which was experimentally determined using size-exclusion chromatography (SEC).
 4 HBP2 was synthesized via rapid one-pot method using an asymmetric ethoxylated
 5 pentaerythritol PP50 core and bis-MPA branching monomer. The skeletal formula of HPB2 is
 6 shown in Figure 1. Perfectly branched second-generation dendrimer, designated hereafter as D2,
 7 was synthesized from bis-MPA branching monomer and symmetric pentaerythritol core through
 8 a divergent growth approach via anhydride coupling as described elsewhere [15]. Note that both
 9 the synthesis of bis-MPa based dendrimers using asymmetric ethoxylated pentaerythritol cores
 10 and HBPs with symmetric pentaerythritol cores were attempted but proved to be too challenging
 11 as yet. The skeletal structure of D2 is also shown in Figure 1. The theoretical (calculated from
 12 chemical structure) molecular weight of D2 is 1529.5 g/mol. Analysis using Matrix-Assisted
 13 Laser Desorption/Ionization Time-of-Flight Mass Spectrometry (MALDI-ToF MS), as shown in
 14 Figure S1 (Supplementary Data), indicated nearly the same molecular weight for D2, i.e. 1528.8
 15 g/mol, thus confirming its unimolecular structure in contrast to the vastly polydisperse HBP2.

1 Synthetic work to prepare dendrimers of higher generations, namely third and fourth, is
2 currently ongoing. The difficulty, however, is producing multigram quantities of the dendrimers
3 required for conducting dilatometric and other bulk tests. Once larger quantities of higher
4 generation dendrimers are available, we plan to extend this comparison study.

5 Films of D2 and HBP2 were prepared by compression molding using a Carver Melt
6 Press. Prior to compression molding, the polymers were first dried for at least 24 hours at 80°C
7 at reduced pressure in a vacuum oven. Then, an appropriate amount of each polymer was placed
8 in a mold which was sandwiched between two Teflon sheets and two metal plates on the outside.
9 The whole construction was placed in the press and preheated at 120°C for 10 min without
10 pressure. Then, the pressure was first increased to 2,500 psi and released, then increased to 5,000
11 psi and released again to remove air bubbles. Finally the pressure was increased to 7,500 psi and
12 held to complete molding, after which the mold was cooled by flowing cold water through the
13 press platens. The molded samples were removed and placed in a desiccant chamber until further
14 testing.

15 In this study HBP2 was also fully (100%) esterified with acetyl chloride, CH_3COCl , to
16 substitute the proton donating hydroxyl groups with acetate groups and thus completely
17 eliminate the ability of this HBP to form H-bonds. Functionalization (esterification) was carried
18 out according to the methodology of alkylation described elsewhere [17]. To fully esterify
19 HBP2, 5.0 g (2.86 mmol) of HBP2 was first dissolved in 40 ml of acetone in a flask. Then, 13.90
20 g triethylamine (137.6 mmol) and 0.30g 4-dimethylaminopyridine (DMAP) (2.4 mmol) were
21 successively added to the flask and mixed with the solution. The flask was cooled to 0°C using
22 an ice-water bath. In parallel, 7.20g liquid acetyl chloride (91.52 mmol) was mixed with 50 ml
23 acetone in a dropping funnel and added to the flask dropwise over 3 hours to initiate the reaction,
24 which then continued overnight until completion. To separate the modified HBP2 from
25 trimethylamine hydrochloride, NaHCO_3 containing water solution (10% wt/wt) was poured into
26 the flask. After phase separation, the bottom liquid layer was enriched with the HPB2-CH_3 ,
27 while the top layer mainly contained the water-salt solution. The bottom liquid layer containing
28 HPB2-CH_3 was collected using a separatory funnel. Importantly, dichloromethane was added to
29 ease the flow of the very viscous polymer enriched phase through the funnel. To further purify
30 the polymer containing phase from NaHCO_3 , HCl water solution (2M) was then added, and the

1 bottom layer containing the polymer phase was again collected. The procedure was repeated
2 until no bubbles formed which indicated that all NaHCO_3 had been removed from the polymer
3 containing phase. Then the polymer containing phase was washed with DI water to remove
4 NaCl , separated, and collected again. The aqueous phase remaining after separation was
5 repeatedly checked using AgNO_3 for Cl^- ions, and when not found, the procedure of purifying the
6 modified polymer from the salts was assumed to be completed. The polymer containing phase
7 was dried by adding MgSO_4 to remove water. The pure product was obtained after evaporation
8 of the remaining traces of acetone and dichloromethane, and resembled a viscous liquid. Fully
9 derivatized HBP2 has been termed HBP2-CH₃ in the manuscript. Schematically, the skeletal
10 formula of HBP2-CH₃ is shown in Figure 1.

11 Experimental Methods

12 ¹H NMR was used for structural characterization of all studied polymers at the atomic
13 level. The spectra were collected using a Varian VXR 300 NMR spectrometer. Before the NMR
14 measurements, the polymers were dried at reduced pressure in a vacuum oven for 12 hours at
15 60°C and then dissolved in DMSO-d6 in an amount of 1% (wt/wt).

16 FTIR was mainly employed to compare the extent to which hydroxyl and carbonyl
17 groups in D2 and HBP2 were engaged in hydrogen bonding. The infrared spectra were collected
18 using a Perkin-Elmer 1600 FTIR spectrometer equipped with a home-made heater. The spectral
19 resolution was 2 cm⁻¹. Thin films on the NaCl plates were prepared by solution casting using
20 acetone. After solvent evaporation, the films were dried at reduced pressure in a vacuum oven
21 for 12 hr at 60°C to remove any traces of acetone and water. The IR data at various temperatures
22 were collected from 4000 to 400 cm⁻¹ and then analyzed via OMNICTM Specta.

23 X-ray diffraction was used to probe and compare the structural order in D2 and HBP2.
24 Samples were tested in vacuum (pressure 1 mbar) using a Rigaku S-MAX 3000 3 pinhole X-ray
25 beam apparatus (Cu K α radiation, $\lambda = 1.542 \text{ \AA}$) which enables generating both SAXS and
26 WAXS data in transmission. For WAXS measurements the sample-to-detector distance was 82.5
27 mm, and the q-range was calibrated using a silver behenate standard. WAXS two-dimensional
28 diffraction patterns were obtained using an image plate with an exposure time of 1 h. The two-
29 dimensional WAXS information was further analyzed using the SAXSGUI software package,
30 which generated integrated WAXS intensity versus 2θ diffraction angle plots.

1 Thermal behavior was investigated by differential scanning calorimetry (DSC) using a
2 TA Instruments DSC Q-100. DSC was used to assess T_g and other thermal transitions. The
3 calibration was carried out using indium and sapphire standards. All samples were dried in a
4 vacuum oven for at least 24 hours at 80 °C prior to testing. Samples were first heated to 200 °C at
5 a rate of 10 °C/min to erase thermal history, quenched to -90 °C at 10 °C/min, and then heated to
6 200 °C at 10 °C/min. The second heating scans were reported.

7 Specific volume versus temperature (30 °C - 120 °C) dependencies at various pressures
8 (PVT data) for D2 and HBP2 were measured by high-pressure dilatometry using a fully
9 automated Gnomix-PVT apparatus (Boulder, CO USA) with mercury employed as a confining
10 fluid. The variation of specific volume was recorded with an accuracy of $\pm 0.002 \text{ cm}^3/\text{g}$. PVT
11 data were collected in an isothermal mode. The pressure at each selected temperature was
12 increased incrementally in 10 MPa steps within the range 10-150 MPa. The pressure during each
13 step was held for 60 sec to allow for equilibrium to be reached before the corresponding specific
14 volume was recorded. It should be mentioned here that the dilatometer design required a pressure
15 of at least 10 MPa to be applied during the experiment in order to guarantee the maximum
16 accuracy. The Tait equation of state [19] was used to extrapolate the experimental data to
17 atmospheric pressure (0.1 MPa). This extrapolation routine is directly built into the Gnomix-
18 PVT-apparatus software. Note, the dilatometer measures the change in specific volume. To
19 convert the change into an absolute value of volume, the sample initial density (the reciprocal of
20 the specific volume) was measured at ambient conditions using the Archimedes' principle. The
21 measurements were conducted using a Mettler Toledo Balance (Model XS-104) equipped with a
22 density kit. Small, 2×2 mm film samples were cut and weighed before and after being immersed
23 in toluene. The density was calculated as follows, $\rho = \frac{W_A}{W_A - W_T} \rho_T$, where W_A and W_T are the
24 sample weight measured in air and toluene, and ρ_T is the density of the toluene, which is 0.870
25 g/cm³. The final density was taken as the average of five measurements. The standard error of
26 the density measurements did not exceed 0.002 g/cm³. The experimentally determined densities,
27 at room temperature, of D2 and HBP2 were 1.307 g/cm³ and 1.285 g/cm³, respectively.

28 RESULTS AND DISCUSSION

29 NMR Data and Analysis

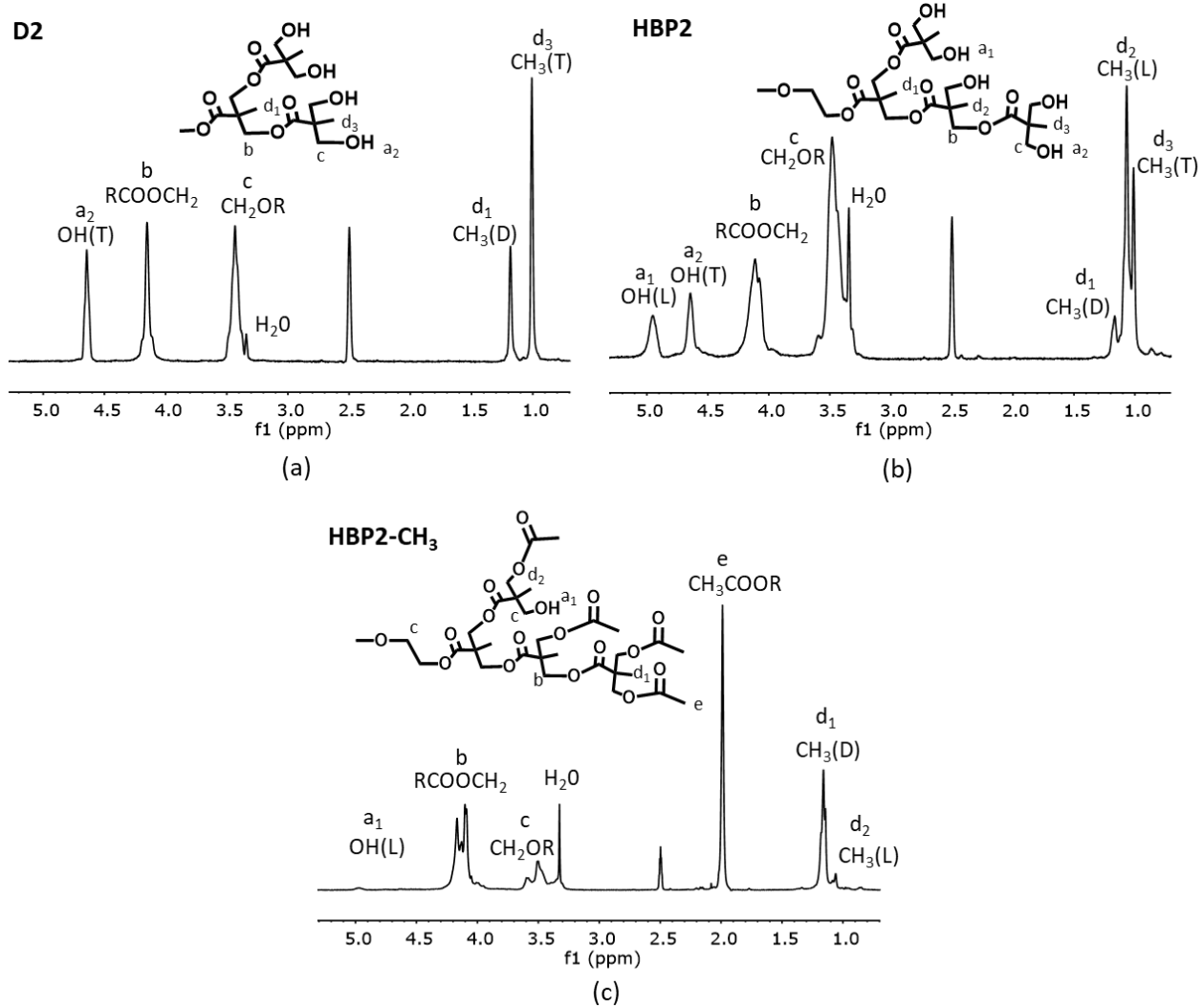


Figure 2 ^1H NMR spectra of (a) D2, (b) HBP2, and (c) HBP2-CH₃ systems.

Figure 2 displays the characteristic ^1H NMR spectra of D2, HBP2, and HBP2-CH₃ systems along with their corresponding peak assignments. As anticipated, for hydroxyl protons the spectrum of D2 revealed only one resonance associated with the terminal hydroxyl units—OH(T)—while the spectrum of HBP2 showed two resonances linked to linear—OH(L)— and terminal—OH(T)—hydroxyls. Furthermore, for methyl protons the spectrum of D2 revealed two resonances associated with dendritic—CH₃(D)—and terminal—CH₃(T)—units, while the spectrum of HBP2 showed three resonances: dendritic—CH₃(D), linear—CH₃(L), and terminal—CH₃(T). In addition, on both spectra one may clearly see the methylene proton resonances associated with ether/alcohol—CH₂OR—and ester—RCOOCH₂—moieties, as well as a small and narrow peak associated with water. NMR peak integrals and important structural

1 parameters calculated from these integrals for D2 and HBP2 are displayed in Table 1 so that this
 2 information for D2 and HBP2 can be compared.

Table 1. Integrated intensities of selected ^1H NMR peaks of D2, HBP2, and HBP2-CH₃ systems and calculated from these integrals structural parameters;

Assignment	D2	HBP2	HBP2-CH ₃
I(CH ₃) _D	12.00	3.86	32.09
I(CH ₃) _L	-	22.16	3.86
I(CH ₃) _T	24.70	10.14	-
I(CH ₂ OR)	32.67	47.69	18.56
I(RCOOCH ₂)	24.35	24.13	54.12
I(OH) _T	16.11	9.56	-
I(OH) _L	-	7.02	0.44
I(CH ₃ COOR)	-	-	42.39
Calculated values			
DB(Frey)	1.00	0.26	-
[OH]/[CO]	1.32	1.37	0.033
n(OH)	15.94	8.30	-
n(CH ₃)	12.10	6.03	-
[OH]/[CH ₃]	1.32	1.38	0.074
\overline{M}_n (g/mol)	1541.6	861.5	-
[OH] (mmol/g)	10.34	9.64	-
[CH ₃] (mmol/g)	7.85	7.01	-
Degree of acetylation	-	-	94.6%

3 The degree of branching (DB) by Frey and Fréchet was calculated based on their
 4 respective definitions as follows [20,21]:

$$5 DB_{Frey} = \frac{2D}{2D+T} = \frac{2 \cdot I(CH_3)_D}{2 \cdot I(CH_3)_D + I(CH_3)_L} \quad (1)$$

$$6 DB_{Fréchet} = \frac{D+T}{D+L+T} = \frac{I(CH_3)_D + I(CH_3)_T}{I(CH_3)_D + I(CH_3)_L + I(CH_3)_T} \quad (2)$$

1 where D, T, and L are the corresponding molar fractions of dendritic, terminal, and the linear
2 units respectively. As anticipated, the DB for D2, based on either above definition, was equal to
3 one while for HBP2 the DB was much lower, i.e. 0.26 (by Frey) and 0.39 (by Fréchet).

4 The hydroxyl/carbonyl ratio for both D2 and HBP2 was calculated directly from the peak
5 integrals associated with hydroxyl and carbonyl groups as follows:

$$6 \frac{[OH]}{[CO]} = \frac{I(OH)}{1/2 \cdot I(RCOOCH_2)} \quad (3)$$

7 Both D2 and HBP2 exhibited very similar OH/CO ratios, i.e. 1.32 and 1.36 respectively.

8 The average number of hydroxyl groups per molecule, $[n(OH)]_{HBP2}$, was determined for
9 HBP2 assuming that one-pot synthesis produces HBP macromolecules with tetrafunctional core,
10 PP50, and also with difunctional core, B2, which are bis-MPA repeat units with unreacted
11 carboxyl groups which serve as core themselves. This effectively increases the number of HBP
12 entities in the system resulting in a smaller number average molecule weight, $\overline{M_n}$, and fewer
13 number of hydroxyl units per HBP molecule than one would have anticipated theoretically
14 assuming full chemical conversion of bis-MPA and that each formed HBP unit contains PP50
15 core. It has been proposed earlier that a one-pot synthesis of BoltornTM bis-MPA based HBPs can
16 result in hyperbranched structures with and without a PP50 core [22]. Subsequently, the
17 following equation was used to calculate n(OH) for HBP2:

$$18 [n(OH)]_{HBP2} = \frac{N(OH)}{N(PP50) + N(B2)} \quad (4)$$

19 Where $N(OH) = 16.58$, $N(PP50) = 0.84$, and $N(B2) = 1.15$ are the equivalent numbers of
20 hydroxyl groups, PP50 tetrafunctional cores, and B2 difunctional cores. The number of hydroxyl
21 groups, $N(OH)$, was determined from the sum of the peak integrals associated with hydroxyl
22 linear and terminal groups, $I(OH)_L + I(OH)_T$. $N(PP50)$ was calculated knowing the equivalent
23 number of methylene groups in the PP50 core structure, $N(PP50) = 1/28 \cdot [I(CH_2OR)$
24 $+ I(RCOOCH_2) - 4/3 \cdot I(CH_3)]$. $N(B2)$ was calculated from the number of unreacted carboxylic acid
25 groups, $N(B2) = N(COOH)_{unreact} = N(OH) - N(OH)_{theor} = N(OH) - [4 \cdot N(PP50) + 1/3 \cdot I(CH_3)]$.
26 Where $N(OH)_{theor}$ is the ‘theoretical’ (ultimate) equivalent number of hydroxyl groups under
27 condition that HBP molecules are formed with tetrafunctional PP50 core only (complete
28 chemical convergence of all bis-MPA hydroxyl groups). Similarly, we used the following

1 equation and NMR data to calculate n(OH) for D2 with pentaerythritol (PE) core. Naturally, ~~no~~
2 all dendrimer structures in this case are expected to have a core.

3 $[n(OH)]_{D2} = \frac{N(OH)}{N(PE)}$ (5)

4 Where N(OH) = 16.11, and N(PE) = 1.01 are the equivalent numbers of hydroxyl groups and PE
5 cores. N(OH) was determined from the peak integral associated with terminal hydroxyl groups,
6 I(OH)_T. N(PE) was calculated from the equivalent number of methylene groups in the PE core,
7 N(PE) = 1/8 · [I(CH₂OR) + I(RCOOCH₂) - 4/3 · I(CH₃)]. As expected, n(OH) for D2 and HBP2 was
8 found to be very different. For D2, it was very close to the theoretical amount (16), but half that
9 for HBP2, i.e. 15.94 versus 8.30, respectively. This difference reflects the fact that only 42% of
10 all HBP entities in HBP2 contain PP50 cores while the remaining species are formed by
11 branching out from the B2, i.e. the bis-MPA monomer itself.

12 As equivalent number of methyl groups, N(CH₃) = I(CH₃)/3, can easily be determined for
13 HBP2 and D2 from the corresponding methyl group related NMR peaks, and knowing the
14 equivalent numbers of PP50, B2, and PE cores it is possible to determine the average number of
15 methyl groups per molecule, [n(CH₃)]_{HBP2} and [n(CH₃)]_{D2}, for HBP2 and D2. The values for
16 [n(CH₃)]_{HBP2} and [n(CH₃)]_{D2} were found to be 6.05 and 12.11, respectively.

17 The number average molecular weight of HBP2, $[\bar{M}_n]_{HBP2}$, was calculated as follows:

18 $[\bar{M}_n]_{HBP2} = \frac{[N(\text{bis-MPA}) - N(B2)] \cdot (M_{\text{bis-MPA}} - M_{H_2O}) + N(\text{PP50}) \cdot M_{\text{PP50}} + N(B2) \cdot M_{\text{bis-MPA}}}{N(\text{PP50}) + N(B2)}$ (6)

19 Where M_{bis-MPA}, M_{H₂O}, and M_{PP50} are the molecular weights of bis-MPA monomer (134.13
20 g/mol), water – the byproduct of this polycondensation reaction (18 g/mol), and PP50 core (356
21 g/mol). Note, N(bis-MPA) = N(CH₃) = 1/3 · I(CH₃). The number average molecular weight of D2,
22 $[\bar{M}_n]_{D2}$, was calculated similarly:

23 $[\bar{M}_n]_{D2} = \frac{[N(\text{bis-MPA})] \cdot (M_{\text{bis-MPA}} - M_{H_2O}) + N(\text{PE}) \cdot M_{\text{PE}}}{N(\text{PE})}$ (7)

24 Where M_{PE} is the molecular weight of the pentaerythritol (PE) core (136 g/mol). As expected,
25 the number average molecular weight of HBP2, 861.5 g/mol, turned out to nearly half that of D2,
26 1541.6 g/mol. The result for D2 is in excellent agreement with both the theoretical (calculated

1 from chemical structure) molecular weight of D2, 1529.5 g/mol, and the molecular weight
2 determined by MALDI-ToF MS, 1528.8 g/mol.

3 Finally, the number of OH and CH₃ groups per unit weight of a polymer [OH] and [CH₃]
4 were calculated for D2 and HBP2 as follows:

5 $[OH] = \frac{n(OH)}{M_n}$ (8)

6 $[CH_3] = \frac{n(CH_3)}{M_n}$ (9)

7 The average concentration of hydroxyl groups, [OH], turned out to be comparable for both
8 systems, i.e. 10.34 mmol/g for D2 and 9.64 mmol/g for HBP2. Furthermore, the average
9 concentration of methyl groups, [CH₃], 7.85 mmol/g and 7.01 mmol/g, were also comparable.

10 The NMR spectrum of HBP2-CH₃ is presented in Figure 3(c). Derivatization with acetyl
11 chloride changed the NMR spectrum of HBP2 considerably. Importantly, the proton signal
12 linked to terminal hydroxyls completely disappeared and only small remnants of the proton
13 signal associated with linear hydroxyls can still be seen, all indicative of virtually complete
14 replacement of the hydroxyl protons with acetate functional groups. The extent of acetylation
15 was determined by ¹H NMR to be 94.6%.

16 FTIR Data and Analysis

17 Figures 3(a) and 3(b) show the FTIR spectra of D2 and HBP2 at 30 °C and 150 °C. The
18 spectra were normalized with respect to the intensity of the smaller peak centered at 2978 cm⁻¹
19 assigned to antisymmetric

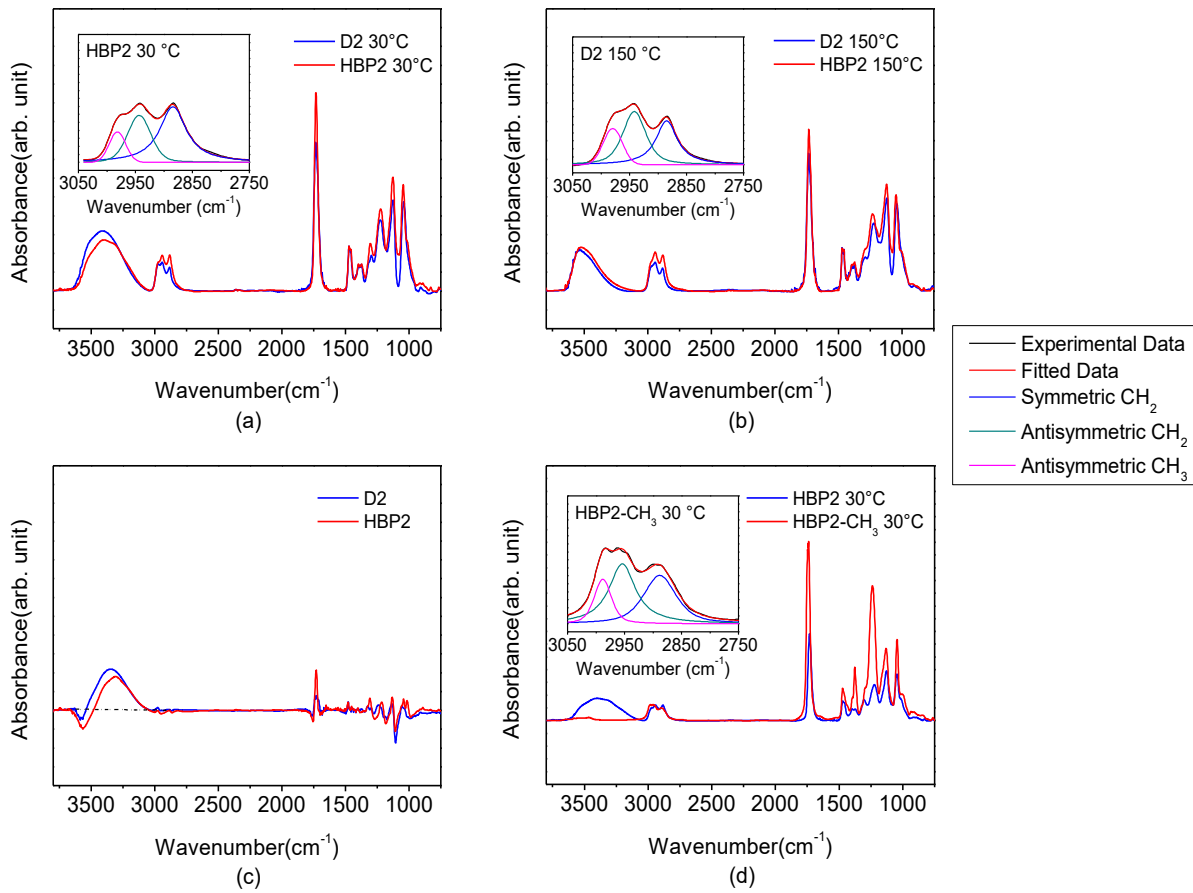


Figure 3 (a) and (b) FTIR spectra of D2 and HBP2 obtained at 30 °C and 150 °C; (c) difference spectra of D2 and HBP2 attained by subtracting the spectra at 150 °C from the spectra at 30 °C; (d) FTIR spectra of HBP2 and HBP2-CH₃ obtained at 30 °C; The insets in (a), (b) and (d) present deconvolutions of methyl and methylene stretching peaks.

1 stretching of methyl groups. This peak was deconvoluted and its intensity was accurately
 2 determined as shown on the inserts to the Figures 3(a) and 3(b). The methyl stretching band was
 3 chosen for normalization because, in contrast to hydroxyl and carbonyl groups, the methyl
 4 groups do not participate in H-bonding, and, as shown in the previous section, the concentration
 5 of these groups in D2 and HBP2 were similar.

6 At 30 °C, both D2 and HBP2 displayed a rather intense and broad asymmetrically shaped
 7 IR band centered at about 3400 cm⁻¹ which was assigned to the stretch vibration of a
 8 combination of free and H-bonded hydroxyl groups (vOH); judging by the pronounced red-shift
 9 of this band, it is predominantly a result of the H-bonded hydroxyls. Note, the reported frequency
 10 range of the free hydroxyl stretch vibration is 3644-3635 cm⁻¹[23,24]. The red-shift of the OH

1 stretch band is due to a reduced force constant and enhanced anharmonicity of the vibrational
2 potential of the O-H oscillator when it participates in H-bonding. Furthermore, the pronounced
3 broadening of this band implies a distribution of various O-H \cdots O associations as a result of the
4 number of donor-acceptor pairs, H-bond angle orientations and lengths; the increase of the band
5 intensity indicates that these associations exhibit a greater dipole moment compared to unbonded
6 hydroxyls [25]. The sharp and intense adsorption peak centered at 1732 cm $^{-1}$ was assigned to the
7 stretching vibration of carbonyl groups (vCO). The reported frequency range of the free carbonyl
8 stretching vibration is 1750-1735 cm $^{-1}$ [26]. Similar to vOH, but to a lesser extent, the vCO band
9 can also be affected by hydrogen bonding-[24,27].

10 One may notice that the intensity of the vOH band for D2 at 30 °C was greater than that
11 for HBP2. Interestingly, the opposite was true with respect to the intensities of the corresponding
12 vCO bands. The peak area ratio at 30 °C, A(vOH)/A(vCO), 2.8 for D2 and 2.3 for HBP2 were
13 found to be greater by about a factor of two than the corresponding hydroxyl to carbonyl group
14 ratios determined by NMR, i.e. 1.32 (D2) and 1.37 (HBP2). This noticeable disagreement
15 implies that in the case of hydrogen bonding the FTIR based hydroxyl/carbonyl peak area ratio
16 does not directly reflect the ratio of the concentrations of these chemical groups and therefore
17 cannot be used for quantitative purposes. The somewhat greater ratio of A(vOH) to A(vCO)
18 observed for D2 versus HBP2 implies that in the former system OH-OH was perhaps a
19 predominant type of H-bond associations with a lesser number of carbonyl groups involved than
20 in the case of HBP2. As expected, upon heating to 150°C, both the vOH peak and vCO peak
21 shifted to higher frequencies, i.e. 3535 and 1734 cm $^{-1}$ (blue-shift), and the corresponding peak
22 intensities were drastically reduced, indicative of the transition from the state with mainly
23 hydrogen bonded hydroxyl and carbonyl groups to the state when they are predominantly free.
24 The blue-shift of the vOH and vCO peaks occur at higher temperature and the transition from
25 predominantly hydrogen bonded to free hydroxyls is particularly apparent when looking at FTIR
26 difference spectra displayed in Figure 3(c) which clearly indicate for both D2 and HBP2 systems
27 the presence of negative (at higher frequencies) and positive (at lower frequencies) differences in
28 the corresponding hydroxyl and carbonyl stretching IR ranges. Interestingly, at 150 °C, the shape
29 and intensity of the vOH and vCO peaks for D2 become comparable with those for HBP2. The
30 A(vOH)/A(vCO) ratios were also calculated for D2 and HBP2 at 150°C to be 1.3 and 1.5
31 respectively, showing similar hydroxyl to carbonyl group ratios as determined by NMR.

1 Figure 3(d) shows a comparison of FTIR spectra at 30°C for HBP2 before and after
2 derivatization with acetyl chloride. The antisymmetric methylene stretching peak at 2945 cm⁻¹
3 (peak deconvolution is shown on the inset) was used for spectrum normalization. As expected,
4 only a very small vOH peak is present after derivatization, and there is a noticeable increase of
5 the peak associated with carbonyl groups.

6 **DSC Data and Analysis**

7 Representative DSC second scans of D2 and HBP2 are shown in Figure 4. Both D2 and
8 HBP2 exhibited a discernible glass transition. Unexpectedly, D2 exhibited a glass transition at

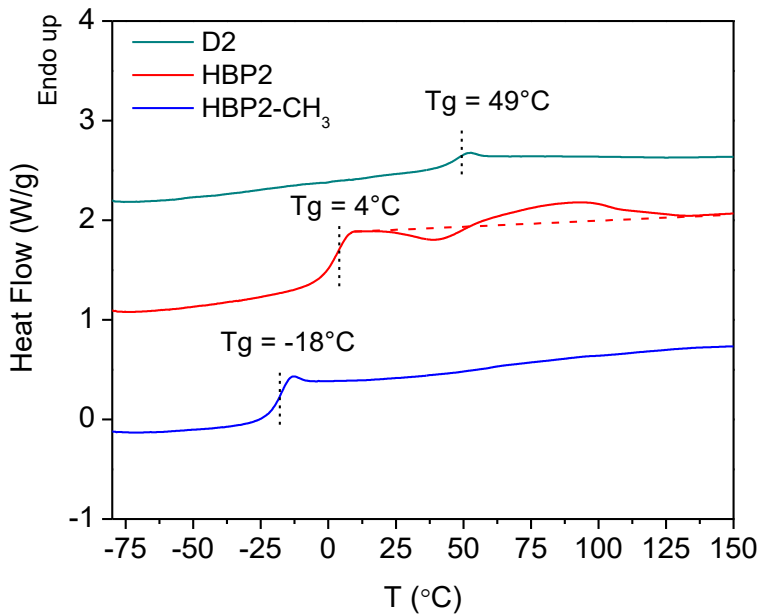


Figure 4 DSC thermograms of D2, HBP2, and HBP2-CH₃ systems

9 noticeably higher temperature than HBP2, 49 °C versus 4 °C, respectively. A question naturally
10 arises regarding the structural factors which can be responsible for this difference in T_g.
11 Thorough experimental analysis of poly(benzyl ether) dendrimers conducted elsewhere
12 suggested that T_g of dendrimers results from two additive contributions. The first term (positive)
13 is defined by the chemical nature of end-group substitution, while the second (negative) is
14 related to the molecular weight of a dendrimer [28]. Therefore, based on the NMR analysis, the
15 large difference in T_g is most likely due to HBP2 having less -- almost by half -- the average
16 molecular weight of D2. Also, HBP2 exhibits a markedly broader molecular weight distribution
17 than D2, with a considerable fraction of low molecular weight products of bis-MPA self-

1 condensation which may additionally contribute to lowering the bulk T_g . Additionally, the
2 presence of two different types of hydroxyl groups, namely linear and terminal hydroxyls, in the
3 HBP2 may also contribute to the reduced bulk T_g . We assume that linear hydroxyls can be more
4 prone to form intramolecular (within dendritic molecules) H-bonds which should affect T_g to a
5 lesser degree than intermolecular (between dendritic molecules) H-bonds which are mainly
6 formed by terminal hydroxyls.

7 As for the other thermal transitions, the DSC measurements of D2 showed only the glass
8 transition, while HBP2 exhibited a more complex behavior. Following the glass transition, one
9 may observe from the DSC thermogram of HBP2 exothermic followed by endothermic events
10 with the corresponding minimum and maximum at about 40 °C and 90 °C. Žagar et al.
11 previously attributed exo- and endo- events in Boltorn™ HBPs to the formation and cleavage of
12 H-bonds and linked specifically to hydroxyl groups of linear (partially esterified) bis-MPA units.
13 It was also suggested that H-bonding between linear units in bis-MPA based HBPs promotes
14 structural ordering which manifests itself via a sharpening and intensification of the major
15 amorphous WAXS halo peak, which has been traditionally linked in polymers to a short-range
16 order between carbon atoms. However, no details regarding the nature of this ordering and how
17 it may lead to a sharpening of the amorphous halo were given. [18,29]

18 Derivatization with acetyl chloride (replacing hydroxyls with acetates), as shown in
19 Figure 4, had a profound effect on the thermal behavior of HBP2. Glass transition temperature
20 decreased by 23 °C from 4 °C to -19 °C. Interestingly, at room temperature, before derivatization
21 HBP2 was a solid and after derivatization the polymer became a viscous liquid. As expected, the
22 exothermic and endothermic events completely disappeared after HBP2 underwent acetylation.

23 **X-ray Data and Analysis**

1 Representative WAXS data of D2 and HBP2, obtained at 25°C and 120°C, are shown in
 2 Figure 5. Note, both D2 and HBP2 samples were dried overnight ~~under~~ in a vacuum oven at
 3 60°C to remove any traces of water before the WAXS measurements were taken (also under

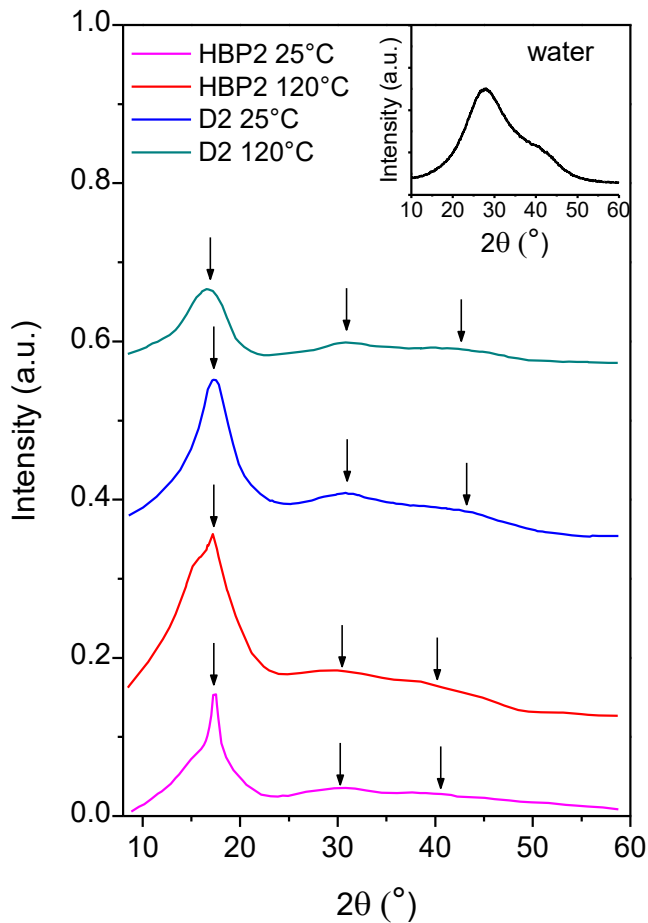


Figure 5 WAXS of D2 and HBP2 systems at 25°C and 120°C. The inset displays WAXS of water at 25°C.

4 vacuum). Both D2 and HBP2 exhibited diffractograms consisting of several peaks, which is
 5 rather uncommon for amorphous polymeric systems. The pattern of D2 at 25°C displayed three
 6 characteristic peaks, a sharper peak at $2\theta = 17.7^\circ$ and two low intensity, broad peaks at $2\theta =$
 7 30.8° and 42° . Angular positions of the peaks at $2\theta = 30^\circ$ and 42° were unaffected by
 8 temperature increase to 120°C. On the other hand, the main halo peak shifted to lower diffraction
 9 angles with temperature, i.e. from $2\theta = 17.7^\circ$ at 25°C to $2\theta = 16.8^\circ$ at 120°C, due to thermal
 10 expansion. Like D2, HBP2 at 25°C exhibited two low intensity, broad peaks at $2\theta = 30^\circ$ and 42° .
 11 The main peak at $2\theta = 17.4^\circ$, however, revealed a somewhat unusual shape in contrast to D2. It
 12 was relatively broad towards the bottom, resembling a typical amorphous halo, and narrower

1 towards the top, reminiscent of peaks typically associated with crystalline and/or ordered
2 structure. Therefore, it was hypothesized that the peculiar shape of the main peak resulted from
3 being composed of two peaks rather than just one. Importantly, heating to 120°C profoundly
4 reduced the intensity of the narrow, order related, peak, indicating that the ordered structure was
5 mostly gone. It is important to note that while the peak intensity was reduced, temperature had
6 no effect on the position of the narrow peak, while the broader amorphous halo part of this
7 combined peak, however, shifted to lower diffraction angles as a result of the thermal expansion
8 of HBP2's bulk structure. Because D2 does not exhibit this ordering behavior, it has been linked
9 to the linear chain segments of partially esterified bis-MPA based HBP. Naturally, we were
10 interested in determining the spatial arrangements of the segments which led to such ordering.
11 Further insight into the structural origin of the narrow WAXS peak was gained by comparison
12 with hydrogen bond mediated mesophase forming systems from the literature. Nylon-6 displays
13 a behavior similar to HBP2, where the sharpness and intensity of the amorphous halo in the X-
14 ray patterns of nylon-6 increases due to the superimposition of a narrow [001] reflection
15 associated with the mesophase on the broader amorphous halo. This [001] reflection in nylon-6
16 has been attributed to a pseudo-hexagonal γ -phase composed of aggregates consisting of parallel
17 and straight, but conformationally disordered chain segments. The H-bonding within these small
18 mesomorphic domains of nylon-6 was considered nearly completed but not restricted to a
19 specific crystallographic direction [30–32]. It is possible that linear units in bis-MPA HBP2 were
20 also able to form a mesophase similar to that found in nylon-6. It is highly likely that the
21 formation of a mesophase is facilitated by H-bonding which can involve both linear hydroxyl
22 and carbonyl groups. We can envisage that morphologically the mesophase exists in the form of
23 small associations which are composed of parallelly arranged short linear segments, the packing
24 of which resembles the hexagonal packing of cylinders. Because of the lacking of
25 conformational order along the segments, the mesophase exhibits lower symmetry as compared
26 to the true crystalline hexagonal order resulting in one major reflection [001]. The relative
27 weakness of other diffraction peaks associated with this packing, for instance [110] and also
28 higher order reflections, perhaps prevent them from being seen against the background of an
29 amorphous halo.

30 Because HBP2 consists of two kinds of hyperbranched macromolecules, namely with
31 four arms growing from the tetrafunctional PP50 core and with two arms growing from the

1 difunctional B2 core (bis-MPA monomer itself) a question can be posed as to what extent both
2 HBP species may contribute to the mesophase formation? Though we don't know the exact
3 answer, the WAXS data obtained elsewhere on different fractions of fourth generation-BoltornTM
4 suggest that lower molecular weight fractions, presumably enriched with the two arm HBP
5 macromolecules, exhibit a greater propensity for ordering as compared to the larger molecular
6 weight fractions [18]. Thus, it is possible that the formation of a mesophase can largely be the
7 prerogative of two-arm HBP molecules, which we believe should have greater translational
8 mobility and less steric constrain, as compared to the four-arm HBP structures.

9 The lower intensity peak at $2\theta \approx 30^\circ$ was present in the scattering intensity patterns of
10 both the bis-MPA HBP2 and its perfect dendritic analog D2; this peak drew our special attention.
11 The inset in Figure 5 displays the WAXS pattern of liquid water. One can see that the main
12 amorphous halo peak of water is at $2\theta \approx 28^\circ$. It is well documented that the three-dimensional
13 hydrogen bond network of water is composed of tetrahedral clusters of H-bonded oxygen and
14 hydrogen atoms and H-bond mediated pair correlation of oxygen atoms within these 3-D H-
15 bonded clusters gives rise to an amorphous halo peak centered at $2\theta \approx 28^\circ$ [33,34]. Because the
16 peak at $2\theta \approx 28^\circ$ on the WAXS patterns of the bis-MPA dendritic polymers is reminiscent of the
17 amorphous halo of water and, furthermore, the hydroxyl groups and water molecules in many
18 aspects are close chemical relatives, we hypothesized that the structural origin of this peak may
19 be related, as it is in water, to the formation of H-bonded clusters of hydrogen and oxygen atoms,
20 O-H \cdots O, and that these clusters may encompass a significant portion of the polymer. Using D2
21 as an example, and considering only carbons and oxygens, the main contributors to X-ray
22 scattering due to their high magnitude of atomic scattering factor, the calculations show that 62%
23 of these atoms are carbons and 38% oxygens. Note that a large portion of these oxygen atoms,
24 i.e. 40%, are within the terminal hydroxyl groups in D2. Therefore, the number of oxygens able
25 to form these O-H \cdots O clusters is truly significant.

1 As hydroxyls are the only proton donating groups in bis-MPA based dendritic structure,
2 converting them to non-hydrogen bonding moieties was an interesting opportunity to see which
3 peaks on the WAXS pattern of HBP2 are directly associated with hydroxyl groups. Figure 6
4 shows the WAXS patterns of HBP2 and fully acetylated HBP2-CH₃. First, the data clearly

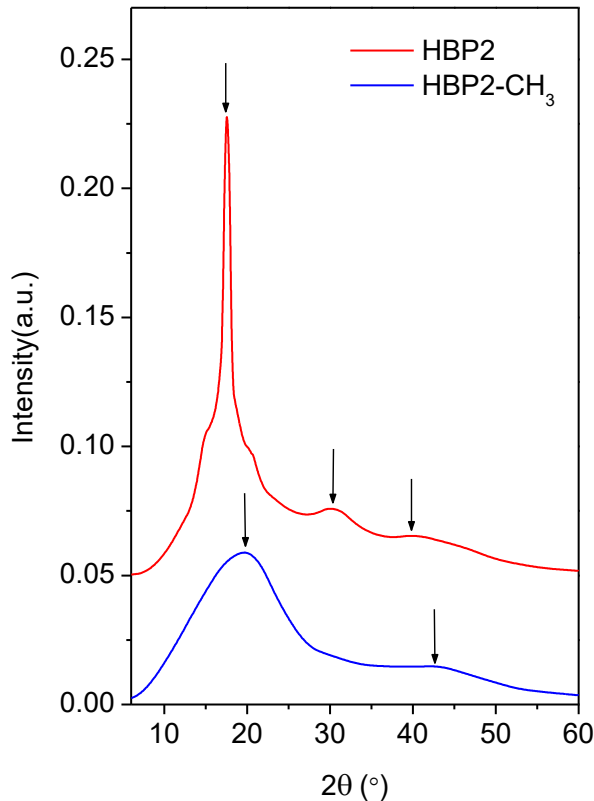


Figure 6 WAXS of HBP2 and HBP-CH₃ systems at 25°C.

5 suggest that there is a direct link between the narrow peak at $2\theta \approx 17^\circ$ and the hydroxyl groups as
6 this peak was absent after acetylation. Furthermore, the broad peak at $2\theta \approx 28^\circ$ was also absent,
7 indicative of its direct link to the hydroxyl groups. The results shown in this section call for more
8 research efforts to shed light on the relationship between H-bonding and structural ordering in
9 bis-MPA based dendritic systems. These efforts are ongoing, and the results will be reported in
10 future communications.

11 **PVT Data and Analysis**

12 The goal of this section was to present the data and analyses of temperature and pressure
13 effects on specific volume of a bis-MPA based perfect dendrimer and its HBP analogue. By

1 analyzing PVT data, first it was planned to understand if there were any volume changes
2 associated with formation or melting of the mesophase in HBP2. Second, it was interesting to
3 determine and compare the thermal expansion, α_m , and compressibility, β_m , coefficients (index m
4 implies the melt state) for D2 and HBP2, and from these coefficients to calculate and compare
5 the internal pressure (energy-volume coefficient), π_T , the thermodynamic parameter directly
6 linked to the magnitude of cohesive forces [35]. The third objective was to attempt fitting the
7 PVT data, obtained for D2 and HBP2 melts, to the Simha-Somcynsky (S-S) equation of state
8 (EOS) to understand if this EOS, originally developed to describe linear polymers, can also be
9 used to describe the PVT surfaces of these dendritic polymers; it has been debated in the past
10 that the S-S approach can generally be used to describe the PVT data of dendritic polymer
11 architectures [36,37]. Note, the poly(benzyl ether) dendrimer polymers are the only systems for
12 which PVT data have been reported and the S-S EOS successfully applied [38,39]. Finally,
13 fitting the experimental data to the theory would have empowered calculating and comparing the
14 fractional free volume, h , in D2 and HBP2 melts.

15 While obtaining PVT data for the acetylated HBP2 system (HBP2-CH₃) was also highly
16 desirable, the liquid state of this system at ambient conditions made it experimentally difficult to
17 accomplish using the Gnomix-PVT apparatus; only solid samples can be loaded into the PVT
18 apparatus.

1 Figure 7 shows the representative specific volume versus temperature dependences at
 2 various pressures for the D2 and HBP2 systems. Note, the samples before PVT measurements
 3 were dried in a vacuum oven at 60°C overnight. The D2 system showed the glass transition
 4 which, as expected, has been gradually shifting to higher temperatures with pressure. So, the
 5 glass transition at 140 MPa for D2 was found ~~at~~ to be 67°C as compared to 49°C (by DSC) at

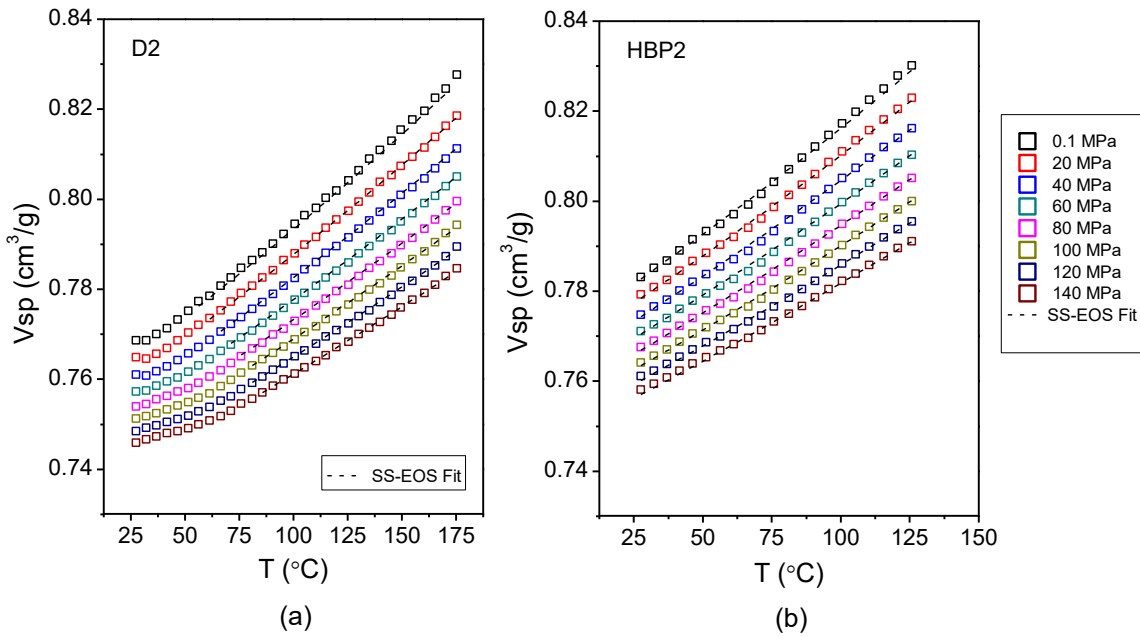


Figure 7 Specific volume versus temperature at various pressures (PVT data) for (a) D2 and (b) HBP2 systems. The dashed lines are obtained by fitting of the Simha-Somcynsky (S-S) EOS to PVT data.

6 atmospheric pressure. Assuming a similar pressure dependence, HBP2 would have shown the
 7 glass transition at about 17°C at 140 MPa, which cannot be observed with this instrument which
 8 operates only at room temperature and above. Indeed, the volumetric measurements of HBP2
 9 showed no glass transition in the studied pressure and temperature range. Neither of the
 10 measurements revealed any measurable changes which would be indicative of any other first or
 11 second order transition, just an ordinary volume thermal expansion behavior. Therefore, the
 12 mesophase, though demonstrable by DSC and WAXS measurements, did not noticeably reveal
 13 itself volumetrically which implies that it has a density similar to the amorphous phase. This also
 14 indicates that the mesophase seems to exhibit only a long range orientational order, similar to the
 15 mesophase in liquid crystalline polymers which are known to display small volume changes

1 associated with a transition to isotropic state as compared to very large volume changes in the
2 case of a true crystalline phase [40].

3 Continuous $V(T)$ and $V(P)$ trends were generated by curve fitting the PVT data to regular
4 polynomials from which the isobaric thermal expansion, $\alpha_m = (\frac{1}{V})(\frac{\partial V}{\partial T})_p$, and isothermal
5 compressibility, $\beta_m = -(\frac{1}{V})(\frac{\partial V}{\partial P})_T$, coefficients in the melt state as a function of temperature
6 were generated for D2 and HBP2. Representative plots of $\alpha_m(T)$ and $\beta_m(T)$ at three pressures
7 0.1, 70, and 150 MPa, covering the studied pressure range, for D2 (closed squares) and HBP2
8 (open triangles) are shown in Figure 8. As expected, the thermal expansion coefficient for both
9 D2 and HBP2 increased with temperature at a given pressure and decreased with pressure at a
10 given temperature, trends which have been typically observed in polymer melts and indicating a
11 link between thermal expansion coefficient in the melt state and the free volume [41]. Thus, at
12 atmospheric pressure (0.1 MPa) and temperature 120°C (this temperature was selected for a
13 comparison) the thermal expansion coefficient of D2 was found to be smaller by about 30% than
14 that of HBP2, i.e. $5.2 \cdot 10^{-4} \text{ K}^{-1}$ versus $6.8 \cdot 10^{-4} \text{ K}^{-1}$, and at 150 MPa this difference was about 26%,

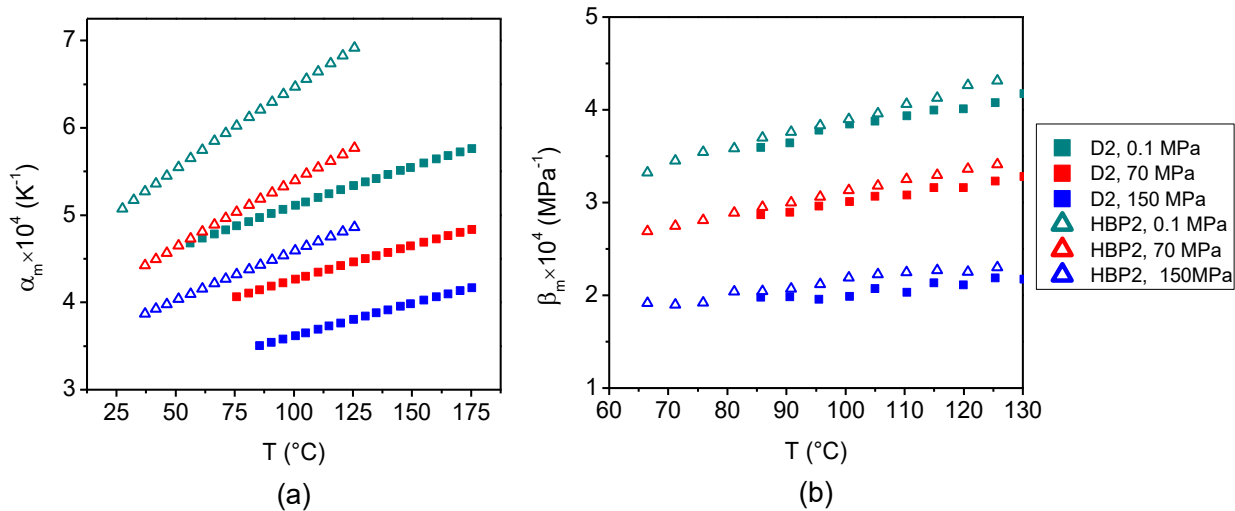


Figure 8 Temperature dependence of the (a) thermal expansion and (b) compressibility coefficient D2 and HBP2 systems at 0.1, 70, and 150 MPa.

15 i.e. $3.8 \cdot 10^{-4} \text{ K}^{-1}$ versus $4.8 \cdot 10^{-4} \text{ K}^{-1}$. The larger thermal expansion coefficient of HBP2 implied
16 that it had a larger free volume than D2. Like thermal expansion coefficients, the compressibility
17 coefficients of D2 and HBP2 increased at a given pressure with temperature and decreased at a

1 given temperature with pressure. The compressibility coefficient of D2 also was slightly smaller
2 than that of HBP2 in line with the trend observed for the thermal expansion. At 120°C and
3 atmospheric pressure the compressibility coefficients of D2 and HBP2 were $4.0 \cdot 10^{-4}$ MPa⁻¹ and
4 $4.3 \cdot 10^{-4}$ MPa⁻¹, and at 150MPa, $2.1 \cdot 10^{-4}$ MPa⁻¹ and $2.3 \cdot 10^{-4}$ MPa⁻¹, respectively.

5 Assuming that both D2 and HBP2 are in the a state of thermodynamic equilibrium when
6 in the melt, the internal pressure, π_T , can be calculated at a given temperature, T, and external
7 pressure, P, from the values of α_m and β_m as this: $\pi_T = \left(\frac{\partial U}{\partial V}\right)_T = \frac{\alpha_m}{\beta_m} \cdot T - P$, where U is the
8 internal energy and V is the volume. The internal pressure is a thermodynamic parameter which
9 allows for estimations of the magnitude of cohesive forces. These forces result in the pressure
10 developed within a liquid or melt which typically falls in the range of 10^2 to 10^3 MPa for various
11 systems at atmospheric pressure [42]. Consequently, π_T of D2 and HBP2 at atmospheric pressure
12 and 120°C were 502.9 MPa and 630.0 MPa, respectively. Two plausible factors leading to the
13 HBP2 system having a larger π_T value than D2 are proposed. First, while HBP2 and D2 display a
14 similar number of polar hydroxyl and ester groups, the former also contains polar ether groups in
15 the core structure. Second, we think that presumably the more globular conformation of D2 may
16 lead to a greater propensity of forming hydroxyl-hydroxyl H-bonds than HBP2, the more open
17 structure of HBP2 allows for enhanced spatial availability of various proton acceptors which
18 may lead to a larger number of hydrogen bonds as a whole both intramolecularly and
19 intermolecularly.

20 Next, we will discuss the results of fitting the PVT data to the Simha-Somcynsky (S-S)
21 equation of state (EOS). The S-S theory belongs to the lattice-hole class of theories [36,37]. The
22 model considers a polymeric system which consists of N linear n -mers each divided into s
23 equivalent segments called s -mers, $sM_s = nM_{rep} = M_n$, where M_s is the molar mass of each s
24 segment, M_{rep} is the molar mass of a monomer repeat unit and M_n is the number average
25 molecular weight of a macromolecule. Each s -mer occupies a cell in the lattice. The s -mers
26 occupy a fraction of the lattice sites, y , while the remaining empty sites are represented by the
27 hole fraction $h(V, T) = (1-y)$. The incorporation of empty lattice sites introduces a disorder into
28 the crystal-like cell structure. The total number of volume-dependent external degrees of
29 freedom is $3c$, and the number of interchain contacts in a lattice of coordination number $z = 12$
30 is $qz = s(z - 2) + 2 \approx 10s$. For longer chains with large s it is typically assumed that $3c/s = 1$.

1 The 6-12 Lennard-Jones (L-J) potential approximates intersegmental interactions, i.e.
 2 interactions between non-bonded segments. The interactions are described in the model by a
 3 maximum attraction energy (minimum in the potential energy plot), ϵ^* , and a repulsion or
 4 segmental hard-core volume, v^* which is calculated from the distance between two segments at
 5 which the intermolecular potential becomes zero. The S-S theory enables calculation of the
 6 partition function assuming random mixing of a specified number of holes and chains followed
 7 by calculation of the Helmholtz configurational free energy, which is presented in terms of
 8 reduced variables, $\tilde{F}[\tilde{V}, \tilde{T}, h(\tilde{V}, \tilde{T})]$. Differentiation of the Helmholtz free energy at
 9 thermodynamic equilibrium results in the S-S EOS which consists of two coupled equations. The
 10 first equation reflects the definition of pressure via free energy, $\tilde{P} = -\left(\frac{\partial \tilde{F}}{\partial \tilde{V}}\right)_{\tilde{T}}$, and the second
 11 results from minimization of the free energy with respect to hole fraction, $\left(\frac{\partial \tilde{F}}{\partial h}\right)_{\tilde{V}, \tilde{T}} = 0$. Below is
 12 the final form of these two equations

$$13 \quad (\tilde{P}\tilde{V})/\tilde{T} = \left[1 - y\left(2^{\frac{1}{2}}y\tilde{V}\right)^{-\frac{1}{3}}\right]^{-1} + y/\tilde{T} \left[2.002(y\tilde{V})^{-4} - 2.409(y\tilde{V})^{-2}\right] \quad (10)$$

$$14 \quad 3c \left[\left(2^{-\frac{1}{6}}y(1/y\tilde{V})^{\frac{1}{3}} - 1/3 \right) / \left(1 - 2^{-\frac{1}{6}}y(1/y\tilde{V})^{\frac{1}{3}} \right) - \right. \\
 15 \quad \left. y(1/y\tilde{V})^2 \left(3.033(1/y\tilde{V})^2 - 2.409 \right) / 6\tilde{T} \right] + (1-s) - s \ln(1-y)/y = 0 \quad (11)$$

16 where $\tilde{P} = P/P^*$, $\tilde{V} = V/V^*$, and $\tilde{T} = T/T^*$ are the reduced variables, and P^* , V^* , and T^* are
 17 the scaling parameters. The scaling parameters are expressed via molecular parameters of the
 18 model as follows, with R the gas constant:

$$19 \quad \left. \begin{aligned} P^* &= zq\epsilon^*/(sv^*) \\ T^* &= zq\epsilon^*/(Rc) \\ V^* &= v^*/M_s \end{aligned} \right\} \left(\frac{P^*V^*}{T^*} \right) M_s = Rc/s \Rightarrow R/3 \quad (12)$$

20 These scaling parameters have been reported for a large number of polymeric systems and enable
 21 formulating the principle of corresponding states in terms of reduced variables for their melts in
 22 a way similar to that formulated for real gases obeying van der Waals equation [43]. We used an
 23 in-house developed computer program which permits calculating the scaling parameters of the
 24 Simha-Somcynsky model after conducting the fitting. The program uses a least square

1 optimization protocol enabling minimization of the chi-square value, $\chi^2 = \sum_{i=1}^N \frac{(M_i - F_i)^2}{\nu_i}$, with
 2 the fit parameters P^* , V^* , and T^* , where M and F are the measured and fit specific volumes,
 3 respectively, and ν is the variance in the measured specific volumes (square of the standard
 4 deviation). The minimization was performed using the MINUIT2 package developed by James
 5 and Roos [44].

6 The S-S EOS fits are shown in Figure 7, along with the experimental data for D2 and
 7 HBP2 polymers. In order to be sure that the S-S EOS fits were all carried out in the melt range,
 8 experimental points 15°C above T_g and greater were only used. The fits were very good, with R
 9 squared values of 0.9999 for both systems, indicating that the S-S EOS allows for an accurate
 10 description of specific volume data for bis-MPA dendritic systems over a broad range of
 11 temperatures and pressures. As the S-S theory is formulated in terms of linear chains, this result
 12 implies that there must exist ‘equivalent’ linear chain representations of D2 and HBP2 dendritic
 13 systems which exhibit the same PVT characteristics. A similar conclusion has been made
 14 previously with respect to poly(benzyl ether) dendrimers [39]. The scaling (characteristic)
 15 parameters, P^* , V^* , and T^* of the S-S model determined for both D2 and HBP2 are listed in
 16 Table 2, along with the values for the molecular parameters of the model, i.e. the segmental
 17 molecular weight, $M_s = \frac{R}{3} \left(\frac{T^*}{P^* V^*} \right)$, the repulsion hard core volume (related to the distance
 18 between two segments at which the intermolecular L-J potential becomes zero), $\nu^* = V^* M_s =$
 19 $\frac{RT^*}{3P^*}$, and the maximum L-J intersegmental attraction energy (minimum in the potential energy
 20 plot), $\varepsilon^* = P^* \nu^* \frac{s}{qz} \approx \frac{1}{10} P^* \nu^* (zq \approx 10s)$.

21 For comparison, the S-S scaling and molecular parameters for polystyrene (PS) and
 22 polyether ether ketone (PEEK), as reported by Rodgers[43], are also included in Table 2.

23 Using this previously reported data set for 56 polymers, the corresponding mean and
 24 standard deviation values for the scaling and molecular parameters have been calculated in our
 25 study which are also reported in Table 2. Furthermore, the table also contains the scaling and

1 molecular parameters for the third (G3) and fifth (G5) generations of poly(benzyl ether)
 2 dendrimers (PBED) reported elsewhere [43]

Table 2. Scaling and molecular parameters of the Simha-Somcynsky (S-S) theory calculated for D2 and HBP2 systems from fitting the PVT data to the S-S EOS in this study. The information for other reported in this Table polymers was obtained from references [39] and [43] . Mean, standard deviation (SD) and relative standard deviation (RSD) were calculated using the data base of S-S parameters for various polymers reported in reference [43];

System	P*(MPa)	V*(cc/g)	T*(K)	M _s (g/mol)	v*(cc/mol)	ε*(kJ/mol)
D2	1144	0.7760	12346	38.54	29.91	3.42
HBP2	1333	0.7747	10708	28.73	22.26	2.97
Mean*	802	0.9506	11216	43.16	40.22	3.11
SD* (RSD*)	157 (19.6%)	0.1689 (17.8%)	1463 (13.0%)	11.97 (27.7%)	10.22 (25.4%)	0.41 (13.2%)
PS*	716	0.9634	12840	51.57	49.68	3.56
PEEK*	1086	0.7705	12580	41.64	32.09	3.49
PBED (G3) [#]	1209	0.8387	11303	30.90	25.92	3.13
PBED (G5) [#]	1209	0.8216	11567	32.28	26.52	3.21

3 *Data from [43]

4 [#]Data from [39]

1 While analyzing the data in Table 2, nothing particularly notable can be seen with respect
2 to T^* , or ϵ^* ($\epsilon^* = \frac{RT^*}{30}$), for either D2 or HBP2. The corresponding values were within a fairly
3 small standard deviation (about 13%) from the mean value calculated using the data set for 56
4 polymers. The same can be concluded for poly(benzyl ether) dendrimers. With that, the T^* and
5 ϵ^* values for D2 were somewhat larger than for HBP2. Because hydrogen bonding interaction is
6 not explicitly considered in S-S model, it is hard to say if this variance can be attributed to the
7 hydrogen bond network difference between the two dendritic bis-MPA based polymers. On the
8 other hand, the P^* scaling parameter values for both D2 and in particular HBP2 systems were
9 significantly greater than the mean value. The scaling parameter P^* is reciprocally proportional
10 to the molecular parameter, $v^* = V^* M_s = \frac{RT^*}{3P^*}$, and since the variance of T^* is generally smaller
11 than P^* , greater values of P^* are typically associated with smaller values of v^* and vice versa, as
12 one may see by comparing the polymers listed in Table 2. Smaller values of v^* (greater P^*) have
13 been previously linked to polymers with oxygen atoms in the backbone, such as linear polyether-
14 ether ketone (PEEK), polysulfone (PSF), polycarbonate (PC), polyethylene terephthalate (PET),
15 and poly(benzyl ether) dendrimers [37]. In contrast to these oxygen containing polymers, carbon
16 chain polymers, like polystyrene (PS) or isotactic polypropylene (i-PP) exhibit noticeably
17 smaller P^* , and fairly large v^* values. It was hypothesized that the oxygen linkages make
18 polymer chains more flexible, which results in smaller values of segmental hard-core volume,
19 v^* . An additional plausible argument beside increased chain flexibility, is the smaller value of
20 the van der Waals radius for oxygen as compared to carbon (1.5 Å vs 1.7 Å). This difference may
21 render more intimate intersegmental contacts leading to smaller v^* . Interestingly enough, both
22 bis-MPA based D2 and HBP2 contain a large number of oxygen atoms in the structure and
23 display larger P^* (smaller v^*). Smaller by 34% the value v^* in HBP2 as compared to D2 was
24 attributed to the fact that the former in addition to ester groups also contained ether groups.
25 Finally, considering that both D2 and HBP2 exhibit similar values of specific volume scaling
26 parameters, V^* , the difference of the segmental molecular weight, M_s , between D2 and HBP2
27 directly reflects the difference in the corresponding segmental hard core volumes, v^* .

28 As it was stated earlier, the important advantage of the S-S theory as compared to many
29 other theories dealing with EOS of polymer melts, is that it allows for the hole fraction
30 (fractional free volume), h , to be extracted from fitting the S-S EOS to PVT data [43]. Figure 9a

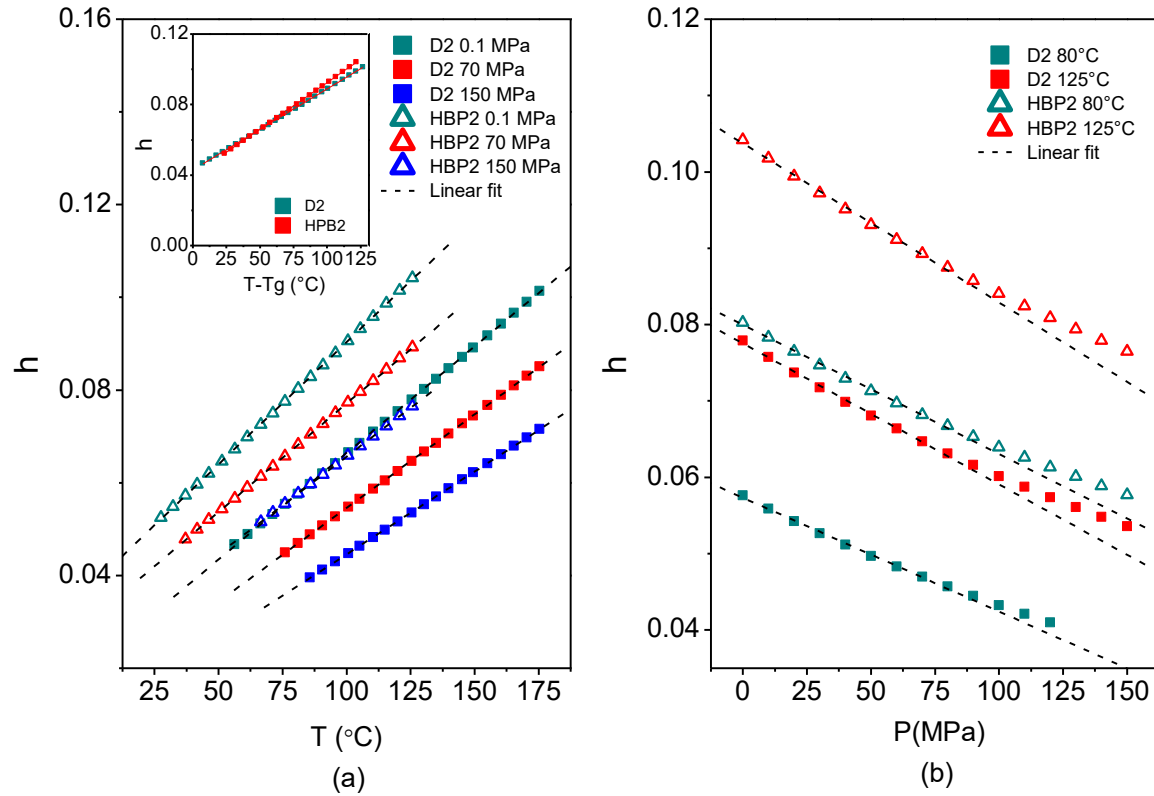


Figure 9 Representative fractional free volume (h) versus (a) temperature and (b) pressure trends for D2 and HBP2 systems. The inset in (a) is the fractional free volume for D2 and HBP2 at 0.1 MPa plotted versus $(T - T_g)$;

1 shows representative plots of fractional free volume, h , versus temperature at three pressures 0.1
 2 MPa, 75 MPa, and 150 MPa. For reference, at atmospheric pressure and 80 °C the respective
 3 fractional free volumes for D2 and HBP2 were 0.057 and 0.079. As expected, the $h(T)$
 4 dependencies were all linear (linear fits are also shown) in accordance with the equation justified
 5 within the free volume theory of glass transition, $h = h_g + \alpha_f(T - T_g)$, where h_g is the
 6 fractional free volume at T_g , and α_f is the thermal expansion of free volume, $\alpha_f = \alpha_l - \alpha_g$, an
 7 α_l and α_g are the thermal expansion coefficients of a polymer in the liquid (melt) and glassy
 8 states at T_g [45,46]. This equation excellently describes the observed difference between the free
 9 volume for D2 and HBP2. The greater T_g of D2 (49° C), as compared with HBP2 (4° C), results in
 10 lower fractional free volume at the same temperature. The inset in Figure 9a shows that the
 11 corresponding fractional free volumes for D2 and HBP2 at atmospheric pressure become
 12 superimposed when plotted as a function of $T - T_g$. The parameters calculated using linear

1 regression applied to the data shown in the inset yield $h_g = 0.040$ and $\alpha_f = 5.3 \cdot 10^{-4} \text{ K}^{-1}$.
2 Interestingly, h_g calculated by linear regression is only 37% larger than the universal value
3 adopted for the WLF equation, $h_g \approx 0.025$, and α_f matches the universal value, $\alpha_f \approx 5.0 \cdot 10^{-4} \text{ K}^{-1}$,
4 even more closely [46].

5 Figure 9b shows the pressure dependence of fractional free volume, $h(P)$, for D2 and
6 HBP2 determined at 80°C and 125°C. It was anticipated that the dependence $h(P)$ at constant T
7 will also be linear as predicted by the free volume theory as follows, $h(P) = f_g + \alpha_f(T - T_g) -$
8 $\beta_f(P - P_0)$ where P_0 is the atmospheric pressure and β_f is the compressibility of free volume,
9 $\beta_f = \beta_l - \beta_g$. Note, the equation describes experimental data for D2 and HBP2 systems
10 reasonably well within 0.1-80 MPa and then the data deviate from the predicted linear trend,
11 presumably due to the fact that β_f is not a constant but a pressure dependent quantity.

12 CONCLUSIONS

13 Both MALDI-ToF MS and ^1H NMR confirmed a monodisperse structure and perfect,
14 1.0, degree of branching for the dendrimer. For the hyperbranched polymer, ^1H NMR revealed a
15 polydisperse structure with a degree of branching that is considerably lower than 1.0, and a lower
16 than expected number average molecular weight due to the concurrent formation of molecules
17 with tetrafunctional core and with difunctional core, i.e. from the bis-MPA monomer itself.

18 Despite structural disparity, the hydroxyl/carbonyl ratio and average concentrations of
19 hydroxyl and methyl groups in the bulk of the two polymers were fairly comparable as
20 confirmed by NMR. FTIR, conducted at elevated temperature, 150°C, (above the transition from
21 the state with mainly hydrogen bonded hydroxyl and carbonyl groups to the state when they are
22 predominantly free) confirmed NMR data and showed similar hydroxyl to carbonyl group ratios
23 for the two polymers. At lower temperature, 30°C, the corresponding hydroxyl to carbonyl group
24 ratios were found noticeably smaller, implying that in the case of strong hydrogen bonding the
25 hydroxyl/carbonyl peak area ratio does not directly reflect the ratio of the concentrations of these
26 chemical groups and therefore cannot be used for quantitative purposes.

27 The glass transition temperature of the HBP was found to be 45°C degrees lower than
28 that of the dendrimer. This large difference was attributed to the HBPs having nearly half the
29 average molecular mass of the dendrimer. Furthermore, HBP exhibits a significantly broader

1 molecular weight distribution, with a considerable fraction of low molecular products of bis-
2 MPA core HBP, which may additionally contribute to lowering the bulk T_g .

3 The unusual shape of the amorphous halo peak at $2\theta \sim 18^\circ$, which was revealed in HBP
4 by WAXS, was attributed to an additional narrow peak superimposed on to the broader
5 amorphous halo. This additional peak was missing on the diffractogram of the dendrimer and so
6 it has been assumed to be the property of bis-MPA HBP only. The structural origin of this peak
7 in HBP was assigned to the temperature-dependent mesophase consisting of small cylindrical
8 aggregates of pseudo-hexagonally packed, H-bonded linear chain segments in HBP. Within these
9 aggregates, chain segments exhibit structural order while lacking conformational order. The
10 lower intensity, broad peak at $2\theta \approx 30^\circ$, present in the X-ray scattering pattern of both the bis-
11 MPA HBP and its dendrimer analog, is due to a large number of hydroxyl groups in the structure
12 of these polymers. It was hypothesized that the structural origin of this peak is related to the
13 formation of H-bonded clusters of hydrogen and oxygen atoms, O-H \cdots O both intramolecularly
14 and intermolecularly, and that these clusters may encompass a significant portion of these
15 polymers.

16 In the melt state, both the dendrimer and the hyperbranched polymer exhibited
17 unremarkable and rather comparable thermal expansion trends without traces of either second or
18 first order transitions. The Simha-Somcynsky (S-S) equation of state (EOS) enabled accurate
19 description of the specific volume data for both bis-MPA systems in a broad range of
20 temperatures and pressures. Successful fitting of PVT data to the S-S EOS permitted obtaining
21 scaling parameters of the S-S theory, and from those calculating the molecular parameters of the
22 model for the dendrimer and HBP. These parameters have been compared with those previously
23 reported elsewhere. Notably, in this comparison, both dendrimer and HBP have exhibited a fairly
24 large value of the scaling parameter P^* (P^* is related to segmental hard-core volume, v^*).
25 Greater P^* (smaller v^*) values have been linked to the presence in the structure of bis-MPA
26 dendritic polymers with oxygen atoms in addition to carbons. Similar tendencies can be seen in
27 other linear polymers containing oxygen atoms in the main chain.

28 The fit of PVT data to the S-S EOS in the melt state enabled the fractional free volume, h ,
29 to be calculated. The temperature dependences of the fractional free volume for both studied
30 polymers exhibited linear trends. When compared at the same temperature and pressure the

1 dendrimer exhibited smaller h than the HBP analogue. This difference was attributed to the T_g
2 difference between two polymers. When h was plotted against $(T-T_g)$ the trends for the two
3 dendritic polymers have superimposed. The pressure dependencies of the fractional free volume
4 also exhibited linear trends but only within limiting pressure range, 0.1 – 80 MPa. At greater
5 pressures a deviation from the linear tendencies was apparent.

6 **Acknowledgments**

7 The authors are grateful to the National Science Foundation-MSN, award #1807096 (SN) and
8 award #1807358 (SMG) for support of this collaborative study. Acknowledgment is also made to
9 the donors of the Petroleum Research Fund administrated by the ACS for support of this
10 research, award #53980-ND7.

11 **Conflict of Interest**

12 The authors declare that they have no known competing financial interests or personal
13 relationships that could have appeared to influence the work reported in this paper.

14

15

16

17

18

19 **REFERENCES**

20 [1] D.A. Tomalia, J.M.J. Fréchet, Discovery of dendrimers and dendritic polymers: A brief
21 historical perspective, *J. Polym. Sci. Part A Polym. Chem.* 40 (2002) 2719–2728.
22 <https://doi.org/10.1002/pola.10301>.

23 [2] D.A. Tomalia, Birth of a new macromolecular architecture: dendrimers as quantized
24 building blocks for nanoscale synthetic polymer chemistry, *Prog. Polym. Sci.* 30 (2005)
25 294–324. <https://doi.org/10.1002/pola.10301>.

26 [3] B.I. Voit, Dendritic polymers: from aesthetic macromolecules to commercially interesting
27 materials, *Acta Polym.* 46 (1995) 87–99. <https://doi.org/10.1002/actp.1995.010460201>.

1 [4] F. Sun, X. Luo, L. Kang, X. Peng, C. Lu, Synthesis of hyperbranched polymers and their
2 applications in analytical chemistry, *Polym. Chem.* 6 (2015) 1214–1225.
3 <https://doi.org/10.1039/c4py01462f>.

4 [5] C. Gao, D. Yan, H. Frey, Promising Dendritic Materials: An Introduction to
5 Hyperbranched Polymers, *Hyperbranched Polym. Synth. Prop. Appl.* (2011) 1–26.
6 <https://doi.org/10.1002/9780470929001.ch1>.

7 [6] Q. Lin, T.E. Long, Polymerization of A2 with B3 monomers: A facile approach to
8 hyperbranched poly(aryl ester)s, *Macromolecules*. 36 (2003) 9809–9816.
9 <https://doi.org/10.1021/ma0257447>.

10 [7] T. Zhang, B.A. Howell, P.B. Smith, Rational Synthesis of Hyperbranched Poly(ester)s,
11 *Ind. Eng. Chem. Res.* 56 (2017) 1661–1670. <https://doi.org/10.1021/acs.iecr.6b04435>.

12 [8] T.H. Mourey, S.R. Turner, M. Rubinstein, J.M.J. Fréchet, C.J. Hawker, K.L. Wooley,
13 Unique Behavior of Dendritic Macromolecules: Intrinsic Viscosity of Polyether
14 Dendrimers, *Macromolecules*. 25 (1992) 2401–2406.
15 <https://doi.org/10.1021/ma00035a017>.

16 [9] S.R. Turner, B.I. Voit, T.H. Mourey, All-Aromatic Hyperbranched Polyesters with Phenol
17 and Acetate End Groups: Synthesis and Characterization, *Macromolecules*. 26 (1993)
18 4617–4623. <https://doi.org/10.1021/ma00069a031>.

19 [10] E. Žagar, M. Žigon, Aliphatic hyperbranched polyesters based on 2,2-
20 bis(methylol)propionic acid - Determination of structure, solution and bulk properties,
21 *Prog. Polym. Sci.* 36 (2011) 53–88. <https://doi.org/10.1016/j.progpolymsci.2010.08.004>.

22 [11] A. Carlmark, E. Malmström, M. Malkoch, Dendritic architectures based on bis-MPA:
23 Functional polymeric scaffolds for application-driven research, *Chem. Soc. Rev.* 42
24 (2013) 5858–5879. <https://doi.org/10.1039/c3cs60101c>.

25 [12] E. Malmström, M. Johansson, A. Hult, Hyperbranched Aliphatic Polyesters,
26 *Macromolecules*. 28 (1995) 1698–1703. <https://doi.org/10.1021/ma00109a049>.

27 [13] H. Magnusson, E. Malmström, A. Hult, Structure buildup in hyperbranched polymers
28 from 2,2-bis(hydroxymethyl)propionic acid, *Macromolecules*. 33 (2000) 3099–3104.

1 https://doi.org/10.1021/ma991100w.

2 [14] H. Ihre, A. Hult, J.M.J. Fréchet, I. Gitsov, Double-stage convergent approach for the
3 synthesis of functionalized dendritic aliphatic polyesters based on 2, 2-bis
4 (hydroxymethyl) propionic acid, *Macromolecules*. 31 (1998) 4061–4068.

5 [15] H. Ihre, O.L. Padilla De Jesús, J.M.J. Fréchet, Fast and convenient divergent synthesis of
6 aliphatic ester dendrimers by anhydride coupling, *J. Am. Chem. Soc.* 123 (2001) 5908–
7 5917. https://doi.org/10.1021/ja010524e.

8 [16] X. Zhang, Modifications and applications of hyperbranched aliphatic polyesters based on
9 dimethylolpropionic acid, *Polym. Int.* 60 (2011) 153–166. https://doi.org/10.1002/pi.2930.

10 [17] E. Malmstrom, M. Johansson, A. Hult, The effect of terminal alkyl chains on
11 hyperbranched polyesters based on 2,2-bis(hydroxymethyl)propionic acid, 197 (1996)
12 3199–3207. https://doi.org/https://doi.org/10.1002/macp.1996.021971012.

13 [18] E. Žagar, M. Huskić, J. Grdadolnik, M. Žigon, A. Zupančič-Valant, Effect of annealing on
14 the rheological and thermal properties of aliphatic hyperbranched polyester based on 2,2-
15 Bis(methylol)propionic acid, *Macromolecules*. 38 (2005) 3933–3942.
16 https://doi.org/10.1021/ma0475434.

17 [19] P. Zoller, PVT relationships and equations of state of polymers, John Wiley & Sons, New
18 York, 1989.

19 [20] D. Höller, A. Burgath, H. Frey, Degree of branching in hyperbranched polymers, *Acta*
20 *Polym.* 48 (1997) 30–35. https://doi.org/10.1002/actp.1997.010480105.

21 [21] C.J. Hawker, R. Lee, J.M.J. Fréchet, One-step synthesis of hyperbranched dendritic
22 polyesters, *J. Am. Chem. Soc.* 113 (1991) 4583–4588.
23 https://doi.org/10.1002/actp.1997.010480105.

24 [22] E. Žagar, M. Žigon, Characterization of a commercial hyperbranched aliphatic polyester
25 based on 2,2-bis(methylol)propionic acid, *Macromolecules*. 35 (2002) 9913–9925.
26 https://doi.org/10.1021/ma021070o.

27 [23] K. Adrjanowicz, K. Kaminski, M. Dulski, M. Jasiurkowska-Delaporte, K. Kolodziejczyk,

1 M. Jarek, G. Bartkowiak, L. Hawelek, S. Jurga, M. Paluch, Dynamic glass transition and
2 electrical conductivity behavior dominated by proton hopping mechanism studied in the
3 family of hyperbranched Bis-MPA polyesters, *Macromolecules*. 47 (2014) 5798–5807.
4 <https://doi.org/10.1021/ma5006155>.

5 [24] E. Žagar, J. Grdadolnik, An infrared spectroscopic study of H-bond network in
6 hyperbranched polyester polyol, *J. Mol. Struct.* 658 (2003) 143–152.
7 [https://doi.org/10.1016/S0022-2860\(03\)00286-2](https://doi.org/10.1016/S0022-2860(03)00286-2).

8 [25] B. Athokpam, S.G. Ramesh, R.H. McKenzie, Effect of hydrogen bonding on the infrared
9 absorption intensity of OH stretch vibrations, *Chem. Phys.* 488–489 (2017) 43–54.
10 <https://doi.org/10.1016/j.chemphys.2017.03.006>.

11 [26] A. V. Iogansen, Direct proportionality of the hydrogen bonding energy and the
12 intensification of the stretching ν (XH) vibration in infrared spectra, *Spectrochim. Acta -*
13 *Part A Mol. Biomol. Spectrosc.* 55 (1999) 1585–1612. [https://doi.org/10.1016/S1386-1425\(98\)00348-5](https://doi.org/10.1016/S1386-1425(98)00348-5).

15 [27] P. Krisanangkura, A.M. Packard, J. Burgher, F.D. Blum, Bound fractions of methacrylate
16 polymers adsorbed on silica using FTIR, *J. Polym. Sci. Part B Polym. Phys.* 48 (2010)
17 1911–1918. <https://doi.org/https://doi.org/10.1002/polb.22066>.

18 [28] P.J. Farrington, C.J. Hawker, J.M.J. Fréchet, M.E. Mackay, The melt viscosity of dendritic
19 poly(benzyl ether) macromolecules, *Macromolecules*. 31 (1998) 5043–5050.
20 <https://doi.org/10.1021/ma970198g>.

21 [29] E. Žagar, M. Huskić, M. Žigon, Structure-to-properties relationship of aliphatic
22 hyperbranched polyesters, *Macromol. Chem. Phys.* 208 (2007) 1379–1387.
23 <https://doi.org/10.1002/macp.200600672>.

24 [30] D. Cavallo, L. Gardella, G.C. Alfonso, G. Portale, L. Balzano, R. Androsch, Effect of
25 cooling rate on the crystal/mesophase polymorphism of polyamide 6, *Colloid Polym. Sci.*
26 289 (2011) 1073–1079. <https://doi.org/10.1007/s00396-011-2428-6>.

27 [31] D. Mileva, R. Androsch, E. Zhuravlev, C. Schick, Morphology of mesophase and crystals
28 of polyamide 6 prepared in a fast scanning chip calorimeter, *Polymer (Guildf)*. 53 (2012)

1 3994–4001. <https://doi.org/10.1016/j.polymer.2012.06.045>.

2 [32] D. Mileva, I. Kolesov, R. Androsch, Morphology of cold-crystallized polyamide 6,
3 Colloid Polym. Sci. 290 (2012) 971–978. <https://doi.org/10.1007/s00396-012-2657-3>.

4 [33] T. Head-Gordon, G. Hura, Water structure from scattering experiments and simulation,
5 Chem. Rev. 102 (2002) 2651–2670. <https://doi.org/10.1021/cr0006831>.

6 [34] P. Jedlovszky, J.P. Brodholt, F. Bruni, M.A. Ricci, A.K. Soper, R. Vallauri, Analysis of
7 the hydrogen-bonded structure of water from ambient to supercritical conditions, J. Chem.
8 Phys. 108 (1998) 8528–8540. <https://doi.org/10.1063/1.476282>.

9 [35] R.P. White, J.E.G. Lipson, Free volume, cohesive energy density, and internal pressure as
10 predictors of polymer miscibility, Macromolecules. 47 (2014) 3959–3968.
11 <https://doi.org/10.1021/ma5005474>.

12 [36] R. Simha, T. Somcynsky, On the Statistical Thermodynamics of Spherical and Chain
13 Molecule Fluids, Macromolecules. 2 (1969) 342–350.
14 <https://doi.org/10.1021/ma60010a005>.

15 [37] L.A. Utracki, R. Simha, Analytical representation of solutions to lattice-hole theory,
16 Macromol. Theory Simulations. 10 (2001) 17–24. [https://doi.org/10.1002/1521-3919\(20010101\)10:1<17::AID-MATS17>3.0.CO;2-B](https://doi.org/10.1002/1521-3919(20010101)10:1<17::AID-MATS17>3.0.CO;2-B).

18 [38] G. Hay, M.E. Mackay, C.J. Hawker, Thermodynamic properties of dendrimers compared
19 with linear polymers: General observations, J. Polym. Sci. Part B Polym. Phys. 39 (2001)
20 1766–1777. <https://doi.org/10.1002/polb.1150>.

21 [39] R. Simha, L.A. Utracki, PVT properties of linear and dendritic polymers, J. Polym. Sci.
22 Part B Polym. Phys. 48 (2010) 322–332. <https://doi.org/10.1002/polb.21893>.

23 [40] G. Rehage, J. Frenzel, Glass Transition and the Glassy State in Isotropic and Liquid
24 Crystalline Polymers., Br. Polym. J. 14 (1982) 173–179.
25 <https://doi.org/10.1002/pi.4980140408>.

26 [41] F. Wang, S. Saeki, T. Yamaguchi, Temperature and pressure dependence of thermal
27 expansion coefficient and thermal pressure coefficient for amorphous polymers, Polymer

1 (Guildf). 38 (1997) 3485–3492. [https://doi.org/10.1016/S0032-3861\(96\)00910-X](https://doi.org/10.1016/S0032-3861(96)00910-X).

2 [42] Y. Marcus, Internal pressure of liquids and solutions, *Chem. Rev.* 113 (2013) 6536–6551.
3 <https://doi.org/10.1021/cr3004423>.

4 [43] P.A. Rodgers, Pressure–volume–temperature relationships for polymeric liquids: a review
5 of equations of state and their characteristic parameters for 56 polymers, *J. Appl. Polym.*
6 *Sci.* 48 (1993) 1061–1080.

7 [44] F. James, M. Roos, Minuit - a system for function minimization and analysis of the
8 parameter errors and correlations, *Comput. Phys. Commun.* 10 (1975) 343–367.
9 [https://doi.org/10.1016/0010-4655\(75\)90039-9](https://doi.org/10.1016/0010-4655(75)90039-9).

10 [45] R. Simha, R.F. Boyer, On a general relation involving the glass temperature and
11 coefficients of expansion of polymers, *J. Chem. Phys.* 37 (1962) 1003–1007.
12 <https://doi.org/10.1063/1.1733201>.

13 [46] D.W. Van Krevelen, K. Te Nijenhuis, *Properties of polymers: their correlation with*
14 *chemical structure; their numerical estimation and prediction from additive group*
15 *contributions*, Elsevier, 2009.

16

17